Importin a3 regulates chronic pain pathways in peripheral sensory neurons

Marvaldi, Letizia; Panayotis, Nicolas; Alber, Stefanie

Marvaldi, L., Panayotis, N., Alber, S., Dagan, S. Y., Okladnikov, N., Koppel, I., Di Pizio, A., Song, D.-A., Tzur, Y., Terenzio, M., Rishal, I., Gordon, D., Rother, F., Hartmann, E., Bader, M., & Fainzilber, M. (2020). Importin a3 regulates chronic pain pathways in peripheral sensory neurons. Science, 369(6505), 842–846. https://doi.org/10.1126/science.aaz5875
Document Version: Accepted

Published Version: https://doi.org/10.1126/science.aaz5875

Science AAAS

Accepted Manuscript

Importin α3 regulates chronic pain pathways in peripheral sensory neurons

Letizia Marvaldi[1], Nicolas Panayotis[1], Stefanie Alber[1,#], Shachar Y. Dagan[1,#], Nataliya Okladnikov[1], Indrek Koppel[1], Agostina Di Pizio[1], Didi-Andreas Song[1], Yarden Tzur[1], Marco Terenzio[1, 2], Ida Rishal[1], Dalia Gordon[1], Franziska Rother[3,4], Enno Hartmann[4], Michael Bader[3,4,5], and Mike Fainzilber[1,*]

Affiliations:

[1]Dept. of Biomolecular Sciences, Weizmann Institute of Science, Rehovot 76100, Israel.

[2]Molecular Neuroscience Unit, Okinawa Institute of Science and Technology, Kunigami-gun, Okinawa 904-0412, Japan.

[3]Max-Delbrück-Center for Molecular Medicine, 13125 Berlin, Germany.

[4]Center for Structural and Cellular Biology in Medicine, Institute of Biology, University of Lübeck, 23538 Lübeck, Germany.

[5]Charité-Universitätsmedizin Berlin, 10117 Berlin, Germany.

[#]Equally contributing authors

*Correspondence to: mike.fainzilber@weizmann.ac.il.

One Sentence Summary:

c-Fos nuclear import by importin α3 regulates neuropathic pain.

Abstract:

How is neuropathic pain regulated in peripheral sensory neurons? Importins are key regulators of nucleocytoplasmic transport. Here we found that importin α3 (KPNA4) can control pain responsiveness in peripheral sensory neurons in mice. Importin α3 knockout or sensory neuron specific knockdown in mice reduced responsiveness to diverse noxious stimuli and increased tolerance to neuropathic pain. Importin α3 bound c-Fos and importin α3 deficient neurons were impaired in c-Fos nuclear import. Knockdown or dominant-negative inhibition of c-Fos or c-Jun in sensory neurons reduced neuropathic pain. *In silico* screens identified drugs that mimic importin α3 deficiency. These drugs attenuated neuropathic pain and reduced c-Fos nuclear localization. Thus, perturbing c-Fos nuclear import by importin α3 in peripheral neurons can promote analgesia.

Main Text:

The importin α subfamily of karyopherins are critical for nuclear import in eukaryotic cells (*1, 2*), and participate in cytoplasmic transport in large cells such as neurons (*3, 4*). Despite overlapping importin specificities (*5, 6*), differential expression profiles and varying cargo affinities enable regulation of specific functions by single importins (*7-15*). We sought to identify neuronal functions of importins by behavioral screens on importin α knockout mice. Importin α3 null animals uniquely exhibited an attenuated response to noxious heat (Figs 1A and S1A-C), and did not show overt coping behavior after capsaicin injection (Fig. S1D-F).

We corroborated these findings by intrathecal injection of AAV9 constructs for acute knockdown or overexpression of importin α3 (Fig. S2). Importin α3 knockdown mice revealed delayed paw withdrawal latency to noxious heat in comparison to mice that received control shRNA (Fig. 1B), without any significant effects on exploratory behaviour or motor coordination (Fig. S3A, B). Specificity of the effects was confirmed by reversal of the phenotype upon importin α3 overexpression in importin α3 knockout mice (Fig. 1C), while conversely shRNA knockdown had no further effect in the knockout background (Fig. S3C). Thus, specific loss of importin α3 attenuates responsiveness to diverse noxious stimuli.

We next evaluated importin α3 in neuropathic pain using the spared nerve injury (SNI) model (*16, 17*) (Fig. S4A, B), with periodic monitoring of mechanosensitivity in wild-type and importin α3 SNI animals over three months. Initial responses were similar in both genotypes and diverged from day 60 onwards. At this later stage, importin α3 null animals exhibited increasing tolerance to SNI, with less hypersensitivity to touch (Fig. 1D) and reduced unevoked paw clenching (Fig. S4C), while wild-type animals did not show any improvement. Similar results were obtained by knockdown of importin α3 prior to induction of SNI (Figs S4D, 1E and S4E). From 60 days post-injury, control shRNA treated SNI mice typically

displayed a spontaneous clenched paw phenotype associated with reduced paw print width in the Catwalk assay, while animals treated with anti-importin α3 shRNA revealed improved gait parameters and reduced paw clenching (Fig. S4E, F). Mechanosensitivity assays showed that the neuropathic pain response developed in a similar manner in control and anti-importin α3 shRNA treated mice up to 60 days after injury. From day 60 onward, importin α3 knockdown animals exhibited a significant recovery of the paw withdrawal reflex, in contrast to controls (Fig. 1E). Thus, both knockout and acute knockdown of importin α3 provides relief from chronic neuropathic pain in the SNI model.

Different cell types can participate in neuropathic pain circuits (*19, 20*). We therefore asked if importin α3 effects on neuropathic pain arise specifically in sensory neurons. To this end we carried out viral transduction of shRNA using AAV-PHP.S, a capsid subtype developed for peripheral neuron specificity (*21*). We verified AAV-PHP.S selectivity by lumbar intrathecal injection, observing specific and efficient transduction of DRG sensory neurons (Fig. S5). We then tested the effects of importin α3 knockdown by AAV-PHP.S delivery of shRNA after SNI induction (Fig. S4D), monitoring both evoked (Fig. 1F) and unevoked (Figs 1G and S4G, Movie S1) responses to neuropathic pain. Both the evoked and spontaneous parameters revealed that sensory neuron-specific knockdown of importin α3 provided relief from neuropathic pain, even when knockdown was initiated after establishment of the pain model.

To gain mechanistic insight on the effects of importin α3 knockout in SNI, we compared dorsal root ganglia (DRG) transcriptomes at one week after injury versus 11 weeks, when pain was significantly alleviated (Fig. 2A and Table S1). The differentially expressed gene-sets revealed signatures for a number of transcription factors affected by depletion of importin α3 (Fig. 2B). Among these, the AP1 family was prioritized for further study because c-Fos is a well-documented marker for pain circuits (*22-24*). Indeed, quantitative analysis of four AP1 target genes after SNI revealed reduced expression of *Syngap1* and *RTL1* in

importin α3 null DRG compared with wild type (Fig. 2C). Indeed, *Syngap1* has been implicated in tactile sensory processing (*25*).

c-Fos features both an importin α binding nuclear localization signal (NLS) and a binding motif for transportin, a distinct nuclear import factor (*26*). Multiple members of both these nuclear import factor families are widely expressed in sensory neurons (*27*). We confirmed importin α3 and c-Fos expression in DRG neurons (Fig. S6A-C), and verified that they interact by proximity biotinylation in transfected N2a cells (Fig. S6D) and proximity ligation assay (PLA) of endogenous proteins in sensory neurons (Fig. 2D, E). Basal c-Fos expression was not changed in importin α3 knockout neurons (Fig. S6E, F). c-Fos immunostaining was mostly nuclear in wild type DRG neurons, while in contrast there was little or no c-Fos nuclear accumulation in importin α3 null neurons (Figs 2F-I and S6A, B, G). Thus, importin α3 is required for c-Fos nuclear accumulation in adult sensory neurons.

The c-Fos inhibitor T-5224 is under investigation for analgesic efficacy (*28*, *29*). We tested the effects of T-5224 by intraperitoneal injection in wild type versus importin α3 null mice. T-5224 treatment increased paw withdrawal latency in response to noxious heat in wild-type mice (Fig. S7A-D), while it had no additional effect beyond the already existing attenuation in importin α3 null animals (Fig. S7C, D). However, T-5224 did ameliorate the paw withdrawal latency in von Frey tests of wild type animals one week after induction of SNI (Fig. S7E), a time point where importin α3 knockout or knockdown still had no effect on SNI responses (Fig. 1). Thus c-Fos perturbation has analgesic effects, and importin α3 may act mainly in the later maintenance stage of neuropathic pain.

To confirm that the AP-1 pathway is required for late stage neuropathic pain, we tested the effects of c-Fos or c-Jun knockdown in the SNI model (Fig. S8). Similarly to the effects of importin α3 depletion, c-Fos knockdown reduced sensitivity to noxious heat (Fig. 3A) without affecting basal mechanosensitivity (Fig. 3B). c-Jun knockdown reduced sensitivity to

both noxious heat and mechanical stimuli (Fig. 3A, B). Comparison of c-Fos, c-Jun and importin α3 knockdowns in the SNI model showed that all three shRNAs significantly attenuated the neuropathic pain response 60-90 days post-injury (Fig. 3C). Furthermore, neuron-specific expression of a dominant-negative form of AP-1 termed A-Fos (*30*) significantly attenuated noxious heat sensitivity without affecting basal mechanosensitivity (Fig. 3D, E), and significantly reduced late-stage neuropathic pain in SNI (Fig. 3F). Thus, AP-1 pathway inhibition attenuates neuropathic pain in the SNI model.

Finally, we carried out an *in silico* screen using the Connectivity Map (CMap) database (*31, 32*) to search for drugs that might target the importin α3 – c-Fos pathway. The screen identified approximately 50 compounds with high CMap scores, 35 of which were not known to affect pain (Fig. 4A and Table S2). We selected three compounds for further analysis - ajmaline, an antiarrhythmic alkaloid, sulmazole, a cardiotonic agent, and sulfamethizole, an antibiotic. Ajmaline did not affect responses to noxious heat, but both sulmazole and sulfamethizole showed efficacy in this assay (Fig. 4B). Both of the latter drugs also provided time and dose-dependent relief at both early and late stages of SNI (Figs. 4C-E and S9A, B), and were as effective in ameliorating response of SNI animals to a noxious mechanical stimulus as knockout or knockdown of importin α3 (Fig. 4F). Finally, both sulmazole and sulfamethizole significantly reduced c-Fos nuclear accumulation in wild type neurons, but did not have any further effect on c-Fos nuclear accumulation in importin α3 null neurons (Fig. S9C-E). Thus, drugs mimicking importin α3 loss phenocopy both the analgesic and c-Fos localization effects observed in importin α3 mutant animals.

Here we have shown that perturbing c-Fos nuclear import by importin α3 in sensory neurons reduces sensitivity to noxious stimuli and provides analgesia specifically in the maintenance phase of neuropathic pain. Direct c-Fos inhibition is effective at both early and maintenance stages of neuropathic pain, suggesting that other modes of c-Fos nuclear import or other

transcription factors may control the early pain response, while importin α3 has a key role for later chronic pain. Very recent studies reported discrimination at spinal circuits level between rapid aversive behavior versus sustained pain responses (*33*), and roles for different cell types in mechanosensitivity and nociception (*19, 20*). Our findings indicate that the locus of importin α3 effects on sustained neuropathic pain is peripheral sensory neurons. The expression profiles and levels of both importin α3 and c-Fos are conserved between mouse and human DRG (*34*), and a recent study reported marked upregulation of AP1 family genes in the DRG of neuropathic pain patients (*35*), highlighting the potential of importin α3 as a new drug target for pain. Chronic pain is currently one of the most common unmet medical needs, due to limited analgesic efficacy of existing drugs, coupled with adverse side effects (*36, 37*). Moreover opioids, which are the most commonly used class of pain drugs, carry multiple risks of tolerance and dependence which can lead to significant levels of abuse (*38*). The vast majority of current targets for drug development in the pain field are ion channels and neurotransmitter receptors, localized at the plasma membrane and the synapse. Importin α3 provides an alternative target both in terms of molecular identity and subcellular localization, offering opportunities for future analgesia development.

References and Notes:

1. Y. Miyamoto, K. Yamada, Y. Yoneda, Importin alpha: a key molecule in nuclear transport and non-transport functions. *J Biochem* **160**, 69-75 (2016).
2. M. Christie *et al.*, Structural Biology and Regulation of Protein Import into the Nucleus. *J Mol Biol* **428**, 2060-2090 (2016).
3. N. Panayotis, A. Karpova, M. R. Kreutz, M. Fainzilber, Macromolecular transport in synapse to nucleus communication. *Trends Neurosci* **38**, 108-116 (2015).
4. M. Terenzio, G. Schiavo, M. Fainzilber, Compartmentalized signaling in neurons: from cell biology to neuroscience. *Neuron* **96**, 667-679 (2017).
5. B. Friedrich, C. Quensel, T. Sommer, E. Hartmann, M. Kohler, Nuclear localization signal and protein context both mediate importin alpha specificity of nuclear import substrates. *Mol Cell Biol* **26**, 8697-8709 (2006).
6. M. T. Mackmull *et al.*, Landscape of nuclear transport receptor cargo specificity. *Mol Syst Biol* **13**, 962 (2017).
7. T. Shmidt *et al.*, Normal brain development in importin-alpha5 deficient-mice. *Nat Cell Biol* **9**, 1337-1338; author reply 1339 (2007).
8. F. Rother *et al.*, Importin alpha7 is essential for zygotic genome activation and early mouse development. *PLoS One* **6**, e18310 (2011).
9. G. Gabriel *et al.*, Differential use of importin-alpha isoforms governs cell tropism and host adaptation of influenza virus. *Nat Commun* **2**, 156 (2011).
10. T. Moriyama *et al.*, Targeted disruption of one of the importin alpha family members leads to female functional incompetence in delivery. *FEBS J* **278**, 1561-1572 (2011).
11. K. Ben-Yaakov *et al.*, Axonal transcription factors signal retrogradely in lesioned peripheral nerve. *The EMBO journal* **31**, 1350-1363 (2012).

12. N. Yasuhara *et al.*, Importin alpha subtypes determine differential transcription factor localization in embryonic stem cells maintenance. *Dev Cell* **26**, 123-135 (2013).
13. N. Panayotis *et al.*, Importin alpha5 Regulates Anxiety through MeCP2 and Sphingosine Kinase 1. *Cell Rep* **25**, 3169-3179 (2018).
14. A. S. Sowa *et al.*, Karyopherin alpha-3 is a key protein in the pathogenesis of spinocerebellar ataxia type 3 controlling the nuclear localization of ataxin-3. *Proc Natl Acad Sci U S A* **115**, E2624-E2633 (2018).
15. K. Dohner *et al.*, Importin alpha1 is required for nuclear import of herpes simplex virus proteins and capsid assembly in fibroblasts and neurons. *PLoS Pathog* **14**, e1006823 (2018).
16. I. Decosterd, C. J. Woolf, Spared nerve injury: an animal model of persistent peripheral neuropathic pain. *Pain* **87**, 149-158 (2000).
17. M. Pertin, R. D. Gosselin, I. Decosterd, The spared nerve injury model of neuropathic pain. *Methods Mol Biol* **851**, 205-212 (2012).
18. S. Shiers *et al.*, Neuropathic Pain Creates an Enduring Prefrontal Cortex Dysfunction Corrected by the Type II Diabetic Drug Metformin But Not by Gabapentin. *J Neurosci* **38**, 7337-7350 (2018).
19. H. Abdo *et al.*, Specialized cutaneous Schwann cells initiate pain sensation. *Science* **365**, 695-699 (2019).
20. X. Yu *et al.*, Dorsal root ganglion macrophages contribute to both the initiation and persistence of neuropathic pain. *Nature Communications* **11**, 264 (2020).
21. K. Y. Chan *et al.*, Engineered AAVs for efficient noninvasive gene delivery to the central and peripheral nervous systems. *Nat Neurosci* **20**, 1172-1179 (2017).
22. R. E. Coggeshall, Fos, nociception and the dorsal horn. *Prog Neurobiol* **77**, 299-352 (2005).

23. P. L. Santos, R. G. Brito, J. Matos, J. S. S. Quintans, L. J. Quintans-Junior, Fos Protein as a Marker of Neuronal Activity: a Useful Tool in the Study of the Mechanism of Action of Natural Products with Analgesic Activity. *Mol Neurobiol* **55**, 4560-4579 (2018).

24. J. Lai *et al.*, Dynorphin A activates bradykinin receptors to maintain neuropathic pain. *Nat Neurosci* **9**, 1534-1540 (2006).

25. S. D. Michaelson *et al.*, SYNGAP1 heterozygosity disrupts sensory processing by reducing touch-related activity within somatosensory cortex circuits. *Nature Neuroscience* **21**, 1-13 (2018).

26. M. Arnold, A. Nath, D. Wohlwend, R. H. Kehlenbach, Transportin is a major nuclear import receptor for c-Fos: a novel mode of cargo interaction. *J Biol Chem* **281**, 5492-5499 (2006).

27. N. Sharma *et al.*, The emergence of transcriptional identity in somatosensory neurons. *Nature* **577**, 392-398 (2020).

28. Y. Aikawa *et al.*, Treatment of arthritis with a selective inhibitor of c-Fos/activator protein-1. *Nat Biotechnol* **26**, 817-823 (2008).

29. H. Makino *et al.*, A selective inhibition of c-Fos/activator protein-1 as a potential therapeutic target for intervertebral disc degeneration and associated pain. *Sci Rep* **7**, 16983 (2017).

30. M. Olive *et al.*, A dominant negative to activation protein-1 (AP1) that abolishes DNA binding and inhibits oncogenesis. *J Biol Chem* **272**, 18586-18594 (1997).

31. J. Lamb *et al.*, The Connectivity Map: using gene-expression signatures to connect small molecules, genes, and disease. *Science* **313**, 1929-1935 (2006).

32. A. J. Mears *et al.*, Mining the transcriptome for rare disease therapies: a comparison of the efficiencies of two data mining approaches and a targeted cell-based drug screen. *NPJ Genom Med* **2**, 14 (2017).

33. T. Huang *et al.*, Identifying the pathways required for coping behaviours associated with sustained pain. *Nature* **565**, 86-90 (2019).

34. P. Ray *et al.*, Comparative transcriptome profiling of the human and mouse dorsal root ganglia: an RNA-seq-based resource for pain and sensory neuroscience research. *Pain* **159**, 1325-1345 (2018).

35. R. Y. North *et al.*, Electrophysiological and transcriptomic correlates of neuropathic pain in human dorsal root ganglion neurons. *Brain* **142**, 1215-1226 (2019).

36. A. S. Yekkirala, D. P. Roberson, B. P. Bean, C. J. Woolf, Breaking barriers to novel analgesic drug development. *Nat Rev Drug Discov* **16**, 545-564 (2017).

37. T. J. Price *et al.*, Transition to chronic pain: opportunities for novel therapeutics. *Nat Rev Neurosci* **19**, 383-384 (2018).

38. P. Skolnick, N. D. Volkow, Re-energizing the Development of Pain Therapeutics in Light of the Opioid Epidemic. *Neuron* **92**, 294-297 (2016).

39. L. Urien *et al.*, Genetic ablation of GINIP-expressing primary sensory neurons strongly impairs Formalin-evoked pain. *Sci Rep* **7**, 43493 (2017).

40. J. P. Golden *et al.*, RET signaling is required for survival and normal function of nonpeptidergic nociceptors. *J Neurosci* **30**, 3983-3994 (2010).

41. S. Nakamori *et al.*, Ephedra Herb extract activates/desensitizes transient receptor potential vanilloid 1 and reduces capsaicin-induced pain. *J Nat Med* **71**, 105-113 (2017).

42. L. Marvaldi *et al.*, Enhanced axon outgrowth and improved long-distance axon regeneration in sprouty2 deficient mice. *Dev Neurobiol* **75**, 217-231 (2015).

43. R. B. Perry *et al.*, Subcellular knockout of importin beta1 perturbs axonal retrograde signaling. *Neuron* **75**, 294-305 (2012).

44. J. N. Crawley, Behavioral phenotyping strategies for mutant mice. *Neuron* **57**, 809-818 (2008).

45. S. Y. Dagan, M. M. Tsoory, M. Fainzilber, N. Panayotis, COLORcation: A new application to phenotype exploratory behavior models of anxiety in mice. *J Neurosci Methods* **270**, 9-16 (2016).

46. O. Söderberg *et al.*, Direct observation of individual endogenous protein complexes in situ by proximity ligation. *Nature Methods* **3**, 995-1000 (2006).

47. K. J. Roux, D. I. Kim, M. Raida, B. Burke, A promiscuous biotin ligase fusion protein identifies proximal and interacting proteins in mammalian cells. *Journal of Cell Biology* **196**, 801-810 (2012).

48. T. C. Branon *et al.*, Efficient proximity labeling in living cells and organisms with TurboID. *Nat Biotechnol* **36**, 880-887 (2018).

49. M. Martin, Cutadapt removes adapter sequences from high-throughput sequencing reads. *EMBnet.journal* **17**, 10-12 (2011).

50. A. Dobin *et al.*, STAR: ultrafast universal RNA-seq aligner. *Bioinformatics* **29**, 15-21 (2013).

51. S. Anders, P. T. Pyl, W. Huber, HTSeq--a Python framework to work with high-throughput sequencing data. *Bioinformatics* **31**, 166-169 (2014).

52. M. I. Love, W. Huber, S. Anders, Moderated estimation of fold change and dispersion for RNA-seq data with DESeq2. *Genome Biology* **15**, 550 (2014).

53. K. J. Livak, T. D. Schmittgen, Analysis of relative gene expression data using real-time quantitative PCR and the 2(-Delta Delta C(T)) Method. *Methods* **25**, 402-408 (2001).

54. M. Mahn *et al.*, High-efficiency optogenetic silencing with soma-targeted anion-conducting channelrhodopsins. *Nat Commun* **9**, 4125 (2018).

Acknowledgments:

We sincerely thank Vladimir Kiss, Tali Shalit, Michael Tsoory and Christian Pritz for excellent professional expertise; Nitzan Korem and Yaniv Levi for technical assistance; and Hongjun Song, Charles Vinson and Viviana Gradinaru for generous gifts of essential plasmids via Addgene. **Funding:** Supported by research grants from the European Research Council (Adv grant Neurogrowth, PoC ChronicPain), the Irwin Green Alzheimer's Research Fund, the Simon Family Foundation and Mr. and Mrs. Lawrence Feis. N.P., I.K. and M.T. were partly supported by Koshland senior postdoctoral fellowships, and N.P. was further supported by the Israeli Ministry of Immigrant Absorption. M.F. is the incumbent of the Chaya Professorial Chair in Molecular Neuroscience at the Weizmann Institute of Science.

Author contributions: Conceptualization: M.F. and L.M.; behavior/pain models: L.M., N.P., S.Y.D., N.O., and S.A.; immunohistochemistry/biochemistry/ data analyses: L.M., N.P., S.A., I.K., A.D.P., D.-A.S., Y.T., M.T., I.R., and D.G.; mouse models: F.R., E.H., and M.B.; writing and revision: M.F. and L.M. with input from all authors; supervision and funding: M.F.; **Competing interests:** L.M. and M.F. have patent applications related to this work (Israeli application 268111, pending; PCT international application in process). **Data and materials availability:** All data is available in the main text or the supplementary materials. RNA-seq datasets are available in the GEO database online (accession # GSE137515). The importin α3 null mouse model is available upon request from M.B.'s laboratory.

Supplementary Materials:

Materials and Methods

Figures S1-S9

Tables S1-S2

Movie S1

References (*39-54*)

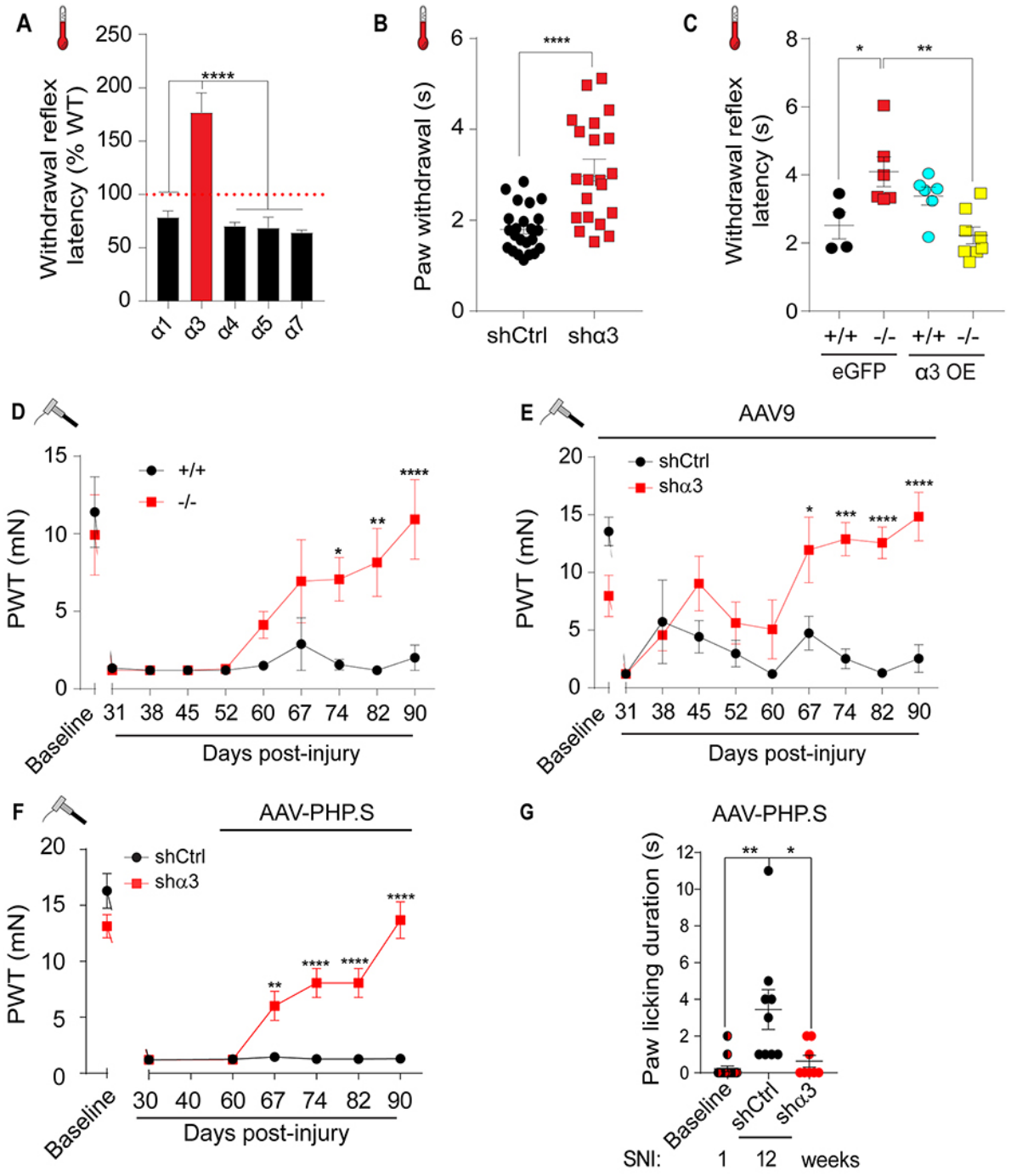

Fig.1. **Attenuated pain responses in importin α3 mice.** (**A**) Importin α3 (α3) are the only line of importin α knockout mice with a higher latency of paw withdrawal in response to noxious heat stimulus (58ºC) compared to wild type littermates. n ≥ 7, **** indicates $p < 0.0001$, one way ANOVA followed by Tukey's multiple comparison test. (**B**) Attenuated response to noxious heat after shRNA-mediated knockdown of importin α3. n = 20, **** indicates $p <$

0.0001, two-tailed unpaired *t*-test. (**C**) Overexpression of importin α3 (α3 OE) restored heat sensitivity in importin α3 knockout animals, while eGFP overexpression had no such effect. n ≥ 4. * indicates $p < 0.05$, ** indicates $p < 0.01$, one way ANOVA followed by Tukey's multiple comparison test. (**D**) Paw withdrawal threshold (PWT) assessed by the von Frey test in SNI animals shows alleviation of long-term neuropathic pain in importin α3 knockout animals. n ≥ 5, * indicates $p < 0.05$; ** indicates $p < 0.01$; **** indicates $p < 0.0001$, two-way ANOVA followed by Sidak's multiple comparison test. (**E**) PWT in SNI animals treated with AAV9 shRNA against importin α3 (shα3) or scrambled control shRNA (shCtrl). n = 7, * indicates $p < 0.05$; *** indicates $p < 0.001$; **** indicates $p < 0.0001$, two-way ANOVA followed by Sidak's multiple comparison test. (**F**) PWT in SNI animals treated with AAV-PHP.S shRNA against importin α3 (shα3) or scrambled control shRNA (shCtrl). n = 9, * indicates $p < 0.05$; ** indicates $p < 0.01$; *** indicates $p < 0.001$, **** indicates $p < 0.0001$, two-way ANOVA followed by Sidak's multiple comparison test. (**G**) Spontaneous (unevoked) paw licking duration measured at 1 week (baseline) and 12 weeks after SNI. n ≥ 9 per group. * indicates $p < 0.05$, ** indicates $p < 0.01$, Kruskal-Wallis followed by Dunn's multiple comparison tests. All quantifications shown as mean ± SEM.

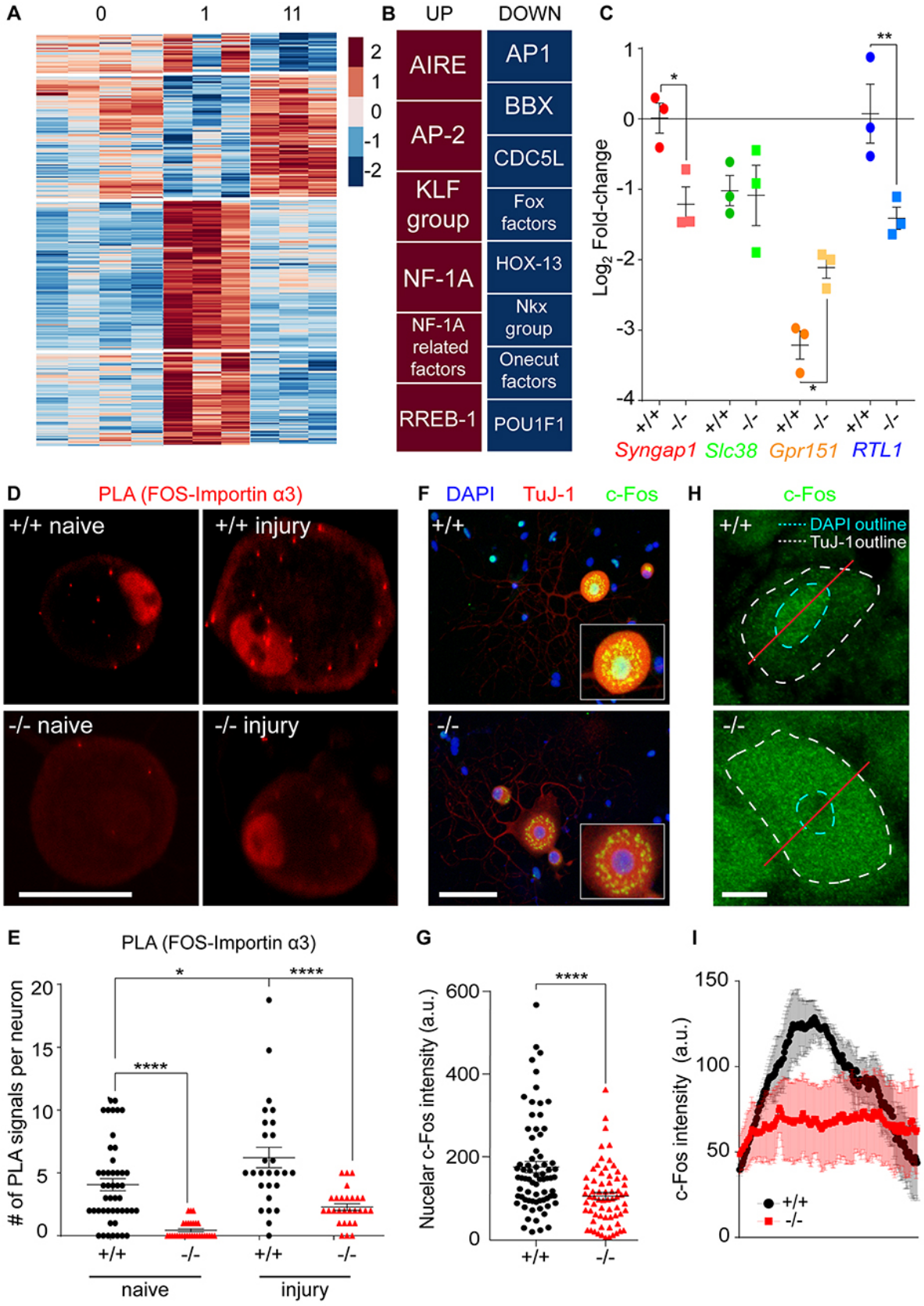

Fig. 2. Transcriptome analyses suggest that c-Fos nuclear import by importin α3 mediates pain responses. (**A**) Heat map of z-score transformed normalized expression values for 530

differentially expressed genes (DEG) at the indicated times (weeks) after SNI in importin α3 null mice (n ≥ 3). (**B**) FMatch (geneXplain) TRANSFAC analyses identify transcription factor (TF) families enriched in DEG promoters from the upregulated (161) and downregulated (369) genes at 11 weeks post-SNI. The AP1 complex was identified as one of the top TF families for the downregulated gene ensemble. (**C**) RT-qPCR analysis of four AP1-target genes, *Syngap1*, *Slc38*, *Gpr151* and *Rtl1*, comparing expression at one versus 11 weeks after SNI in wild-type and importin α3-/- DRGs. n=3, * indicates $p < 0.05$, ** indicates $p < 0.01$, one-way ANOVA followed by Sidak's multiple comparison test. (**D**) Proximity ligation assay (PLA) for c-Fos and importin α3 in CGRP positive DRG neurons fixed after 24 hr in culture from both naive and injury groups. PLA signals shown in red. Scale bar 30 μm. (**E**) Quantification of PLA signals per neuron. n ≥ 29 neurons per group from three independent experiments, **** indicates p <0.0001,* indicates $p < 0.05$, ANOVA followed by Tukey's multiple comparison test. (**F**) Reduced nuclear localization of c-Fos in cultured importin α3 null DRG neurons versus wild type. Scale bar 50 μm. (**G**) Quantification of nuclear c-Fos intensity from the experiment shown in F. n > 67 neurons from 3 independent experiments, **** indicates p <0.0001, two-tailed unpaired *t*-test. (**H**) Reduced nuclear localization of c-Fos in DRG neurons from sectioned ganglia of importin α3 null compared to wild type mice. Cell body and nucleus boundaries determined by Tuj-1 and DAPI staining as indicated (see also Fig. S6G). Scale bar 10 μm. (**I**) Quantification of c-Fos immunofluorescence along line scans as shown in H, n > 206 neurons from three independent experiments. All data are shown as mean ± SEM.

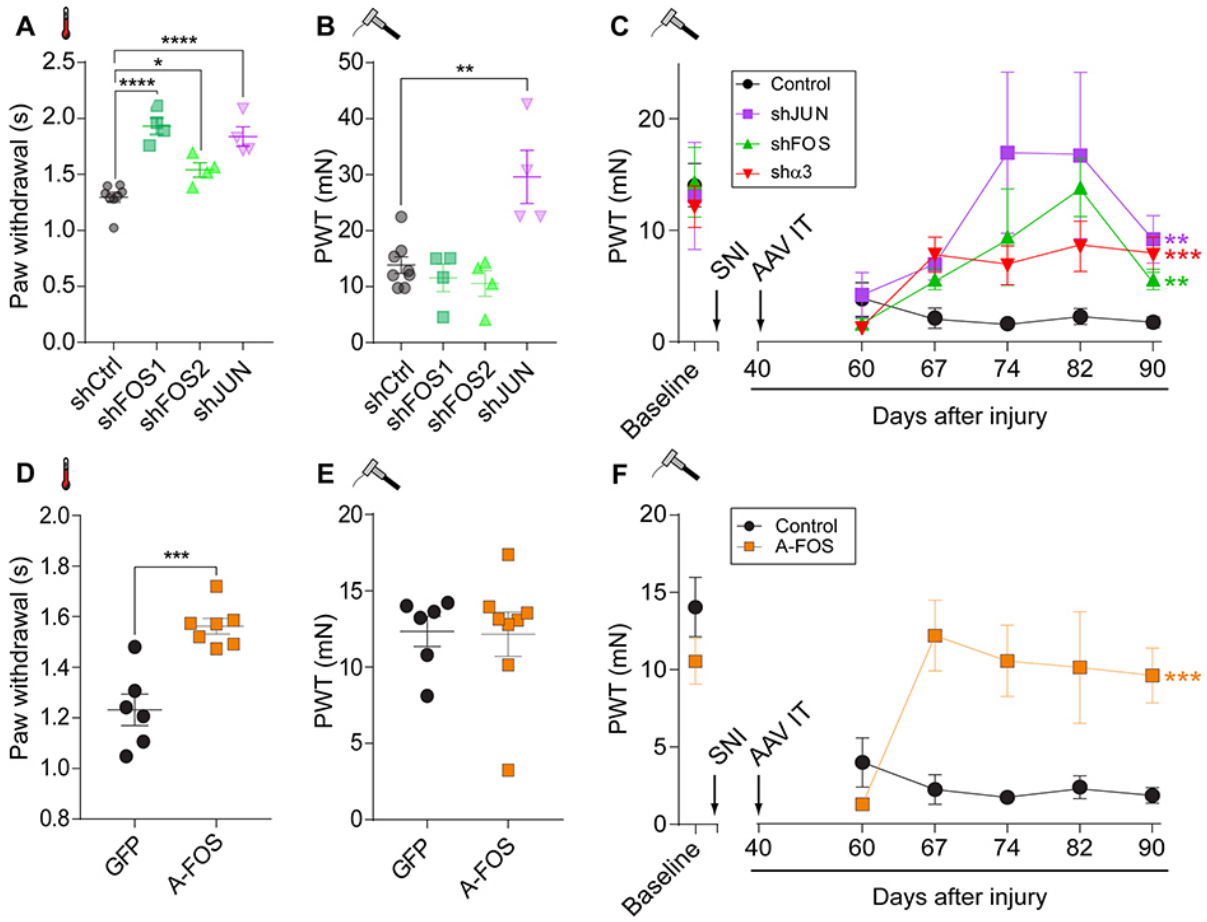

Fig. 3. Acute knockdown or dominant-negative inhibition of AP-1 transcription factors attenuates chronic pain after SNI. (**A**) Reduced noxious heat responses in mice after intrathecal AAV9 delivery of shRNAs targeting c-Fos (shFOS1, shFOS2) or c-Jun (shJUN). n ≥ 4. * indicates $p < 0.05$, *** indicates $p < 0.001$, **** indicates $p < 0.0001$, ANOVA followed by Dunnett's multiple comparison test. (**B**) Reduced mechanosensitivity in shJUN, but not shFOS, treated animals. n ≥ 4, ** indicates $p < 0.01$, ANOVA followed by Dunnett's multiple comparison test. (**C**) Paw withdrawal threshold (PWT) assessed by the von Frey test in SNI animals treated with the indicated shRNAs (shFOS indicates a mixture of both). n ≥ 5, ** indicates $p < 0.01$, *** indicates $p < 0.001$, two-way ANOVA. (**D**, **E**) AAV9 overexpression of the A-Fos dominant-negative (DN) under the neuron-specific human SynapsinI promoter reduces noxious heat responses (D) without effects on basal mechanosensitivity (E), n ≥ 6, two-tailed unpaired t-test. (**F**) PWT in SNI animals treated with the A-Fos dominant-negative

(DN) construct. n ≥ 6, two-way ANOVA. Asterisks indicate significant treatment effects between the groups. ** indicates $p < 0.01$, *** indicates $p < 0.001$. All data shown as mean ± SEM.

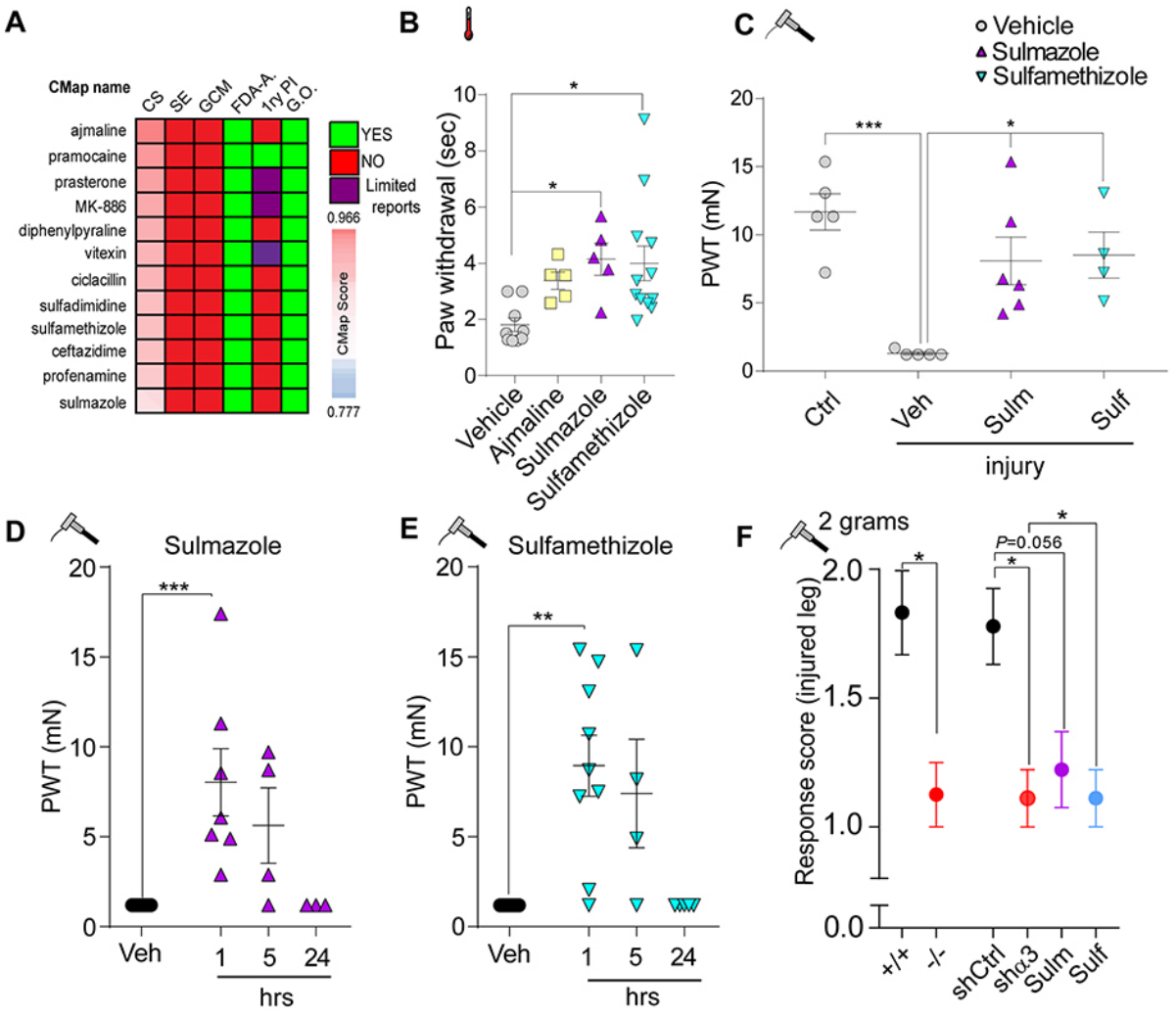

Fig. 4. An *in silico* screen for mimics of transcriptional effects of importin α3 loss reveals new candidate analgesics. (**A**) Impα3 KO DEG lists were used to query CMap for small molecules with similar effects on cell line transcriptomes. Compounds with CMap scores (CS) >0.85 are shown. Compounds were further filtered for minimal predicted side effects (SE), lack of general cell modifying effects (GCM), FDA approved status (FDA-A), and whether or not their primary therapeutic indication (PI) is pain-related. (**B**) Three candidates meeting the desired criteria were tested *in vivo* for effects on response to noxious heat 1 hour after i.p. injection. Sulmazole (0.5 mg/kg, n=5) and sulfamethizole (1.25 mg/kg, n=12) showed significant effects as compared to vehicle (5% DMSO in PBS, n=9), while ajmaline (1 mg/kg, n=5) did not. (**C**) Significant effects of sulmazole (1.25 mg/kg, n=6), and sulfamethizole (3.12 mg/kg, n=4) compared to vehicle (5% DMSO in PBS, n=5) in the SNI model of neuropathic

pain. Drugs were tested 60 days after establishing the model by two i.p. injections with 1 week interval, followed by von Frey tests 1 hr after the second injection. Ctrl is the uninjured leg. ANOVA followed by Sidak's multiple comparison test, * indicates $p < 0.05$, *** indicates $p < 0.001$. (**D-E**) Duration of drug effects one week after SNI, with von Frey tests performed 1, 5 and 24 hr after i.p. injection. $n \geq 4$, Kruskal-Wallis test followed by Dunn's multiple comparison test, ** indicates $p < 0.01$, *** indicates $p < 0.001$. (**F**) Noxious mechano-sensitivity testing of SNI mice treated as shown, using von Frey filaments of 2 grams force. Scoring from 0 to 2, with 0 = no response, 1 = signs of discomfort, 2 = withdrawal of the leg. $n \geq 6$, Kruskal-Wallis test followed by Dunn's multiple comparison test, * indicates $p < 0.05$. Data shown as mean ± SEM throughout.

Science
AAAS

Supplementary Materials for

Importin α3 regulates chronic pain pathways in peripheral sensory neurons

Letizia Marvaldi[1], Nicolas Panayotis[1], Stefanie Alber[1,#], Shachar Y. Dagan[1,#], Nataliya Okladnikov[1], Indrek Koppel[1], Agostina Di Pizio[1], Didi-Andreas Song[1], Yarden Tzur[1], Marco Terenzio[1, 2], Ida Rishal[1], Dalia Gordon[1], Franziska Rother[3,4], Enno Hartmann[4], Michael Bader[3,4,5], and Mike Fainzilber[1,*]

Correspondence to: mike.fainzilber@weizmann.ac.il

This PDF file includes:

Other Supplementary Materials for this manuscript include the following:

Materials and Methods

Mice

All animal experiments were reviewed and approved by the Institutional Animal Care and Use Committee (IACUC) at the Weizmann Institute of Science. Importin α single gene knockouts for importin α1, α3, α4, α5 and α7 were generated by conventional gene deletion strategies (*7-9, 15*). C57BL/6 mice were from Envigo Ltd (Israel). All mouse strains used were bred and kept at 24 °C in a humidity-controlled room under a 12 hr light–dark cycle with free access to food and water. Experiments were carried out on animals between 2-5 months old.

Noxious stimuli and pain models

The initial screen for responses to noxious heat was conducted by applying a metal probe heated to 58ºC to a hindlimb paw, while holding the animal. Paw withdrawal latency was timed, typically ranging between 2-4 seconds in wild-type animals. If the paw is not withdrawn within 20 seconds the assay is terminated. The test was repeated three times for each animal, with at least 20 minute intervals between repeats.

We also assessed heat sensitivity using the hot plate test (*39*). To do so, mice were placed individually in a 20 cm high Plexiglas box on a metal surface set at 52, 55 or 58ºC, and the latency to initiate a nociceptive response (licking, hind paws shaking, jumping) was monitored by videotape. Mice were removed from the plate immediately after a nociceptive response.

The behavioral response to cold stimulation was tested using the acetone evaporation test (*40*). In brief, acetone (100%, 70 µl) was applied twice onto the plantar surface of the hind paw using a micropipette with an interval of 20 min between each application. Animals were then videotaped for one minute and the latency to initiate hind paw licking was measured.

We further assessed acute pain related behaviours induced by plantar injection of 50 µg/kg capsaicin (Sigma Aldrich, M2028) into the hind paw as previously described (*41*). Mice were placed in a transparent cylinder and video recorded for three minutes after the injection. Paw licking time and latency were measured in seconds.

We assessed chronic neuropathic pain using the spared nerve injury (SNI) model (*16*). Mice were anaesthetized with Ketamine/Xylazine (10 mg/kg body weight, IP injection). The skin on the lateral surface of the thigh was incised and a section made directly through the biceps femoris muscle in order to expose the sciatic nerve and its three terminal branches: the sural, common peroneal and tibial nerves. The SNI procedure comprised an axotomy and

ligation of the tibial and common peroneal nerves leaving the sural nerve intact. The peroneal and the tibial nerves were tightly ligated and cut distal to the ligation. The lesion results in a marked hypersensitivity in the lateral area of the paw innervated by the spared sural nerve. Mice were investigated over a period of three months.

Behavioral Tests

All assays were performed during the "dark" active phase of the diurnal cycle under dim illumination (~10 lx) unless otherwise stated; the ventilation system in the test rooms provided a ~65 dB white noise background. Every daily testing session started with one hour habituation to the test rooms. A recovery period of at least one day was provided between the different behavioral assays. Animals were marked with transient dye labels on the tails to enable blinded testing.

von Frey tests of sensitivity to mechanical stimuli were conducted as previously described (*42*). Briefly, mice were placed in acrylic chambers suspended above a wire mesh grid and allowed to habituate to the testing apparatus for one hour prior to experiments. When the mouse was calm, the von Frey filaments were pressed against the plantar surface of the paw until the filament buckled and held for a maximum of 3 seconds. A positive response was noted if the paw was sharply withdrawn on application of the filament. Testing began with filament target force 13.7 milliNewtons and progressed according to an up-down method (*42*). 2 gram von Frey filaments were used to assess sensitivity to noxious mechanical stimulation, scoring mice responses as follows: 0, no response; 1, visible signs of discomfort without leg withdrawal; 2, withdrawal of the leg.

CatWalk gait analysis and training was carried out as previously described (*43*). Motivation was achieved by placing the home cage at the end of the runway. The test was repeated at least three times for each mouse. Data were collected and analyzed using the Catwalk Ethovision XT11 software (Noldus Information Technology, The Netherlands).

We carried out rotarod experiments to assess integrity of balance and coordination (*44*) using a ROTOR-ROD™ system (83x91x61 - SD Instruments, San Diego). Mice were subjected to three trials with 20 minutes inter-trial intervals over three consecutive days at three weeks and five weeks after AAV9 injection, calculating the daily average each time. Rotarod acceleration was set to 20 rpm in 240 sec. Latency to fall (sec) was recorded and the average of six consecutive trials was used as an index of motor coordination and balance.

Motility and anxiety-like behaviors were assayed in the open field (OF) as previously described (*13*). Mouse activity was tracked and recorded using VideoMot2 (TSE System,

Germany). OF was performed under 120 lx for the assessment of anxiety-related behaviors. OF raw data were further analyzed with *COLOR*cation (*45*).

Pain coping behavior was monitored by quantification of paw licking of the injured limb, recording mouse activity over a period of 10 minutes inside a transparent enclosure (15 x 29 x 12 cm) containing a ~1 cm layer of cage litter. Recording was conducted using a high-resolution GigE camera directly connected to Noldus Media Recorder software (Noldus, Wageningen, the Netherlands), collecting both top and lateral views in the same video by positioning a 45º angle mirror above the cage. We quantified spontaneous licking of the SNI-injured paw at one week after SNI and in both AAV-PHP.S-shCtrl and AAV-PHP.S-shα3-injected mice 12 weeks after the injury. Recordings were analyzed off-line in a blinded manner to determine accumulative paw licking duration during the recording period.

Histology

Lumbar sections of the spinal cord including DRGs were pre-fixed for 6 minutes before dissection of spinal cord and associated DRGs. Lumbar DRG (L4, unless otherwise indicated) and/or spinal cord were then fixed for six hours in 4% PFA in PBS, washed in PBS and cryoprotected in 20% w/v sucrose in PBS before serial cryo-sectioning at a thickness of 10-20 µm. One set for each DRG was then processed for immunostaining. Briefly, sections were rehydrated in PBS, blocked and permeabilized with 15% Donkey Serum, 5% BSA, 0.3% Triton X-100 in PBS for 3 hours and incubated with Mouse anti-βIII tubulin (Abcam ab18207, IF TuJ1, 1:1000), Rabbit anti-cFos (Millipore Ab5 4-17, IF 1:500), Mouse anti-cFOS (Millipore Ab5 4-17, IF 1:500), Mouse anti-Jun (BD transduction Laboratories, IF 1:1000), Rabbit TRPV1 (Alomone ACC-030, 1:500), Rabbit anti-GFP (Abcam ab6556, IF 1:1000 or WB 1:500), Goat anti-CGRP (AbD SEROTEC 1720-9007, IF 1:1000), MBP (Abcam ab7349, IF 1:500) or Rabbit anti-importin α3 (1:2000, Michael Bader lab', MDC Berlin) antibodies overnight at 4°C. On the following day sections were washed three times in PBS before incubation for two hours with different combinations of donkey anti-chicken/rabbit/mouse secondary antibodies (Alexa Fluor 647, 594, 488; Jackson Immunoresearch, 1:1000). Coverslips or slides were then washed and mounted with Fluoromount-G™.

Image processing

Images were acquired on a confocal laser-scanning microscope (Olympus FV1000, 60x oil-immersion objective Olympus UPLSAPO - NA 1.35) using Fluoview (FV10–ASW 4.1) software. DRG sections were scanned using camera settings identical for all genotypes in a

given experiment. Images from high-resolution confocal z-stacks were imported into the *Fiji* version (http://fiji.sc) of *ImageJ* for background subtraction and subsequent analyses as detailed below.

Fluorescence Intensity Analysis: Line scan analyses of fluorescence intensity were carried out on DRG tissue sections to determine fluorescence intensity of c-Fos and importin α3 over cell regions of interest in vivo. Signal in the channel of interest was quantified along each line scan, and all collected traces were averaged for each experimental group. For comparison of nuclear and cytoplasmic staining intensity we processed 8-bit images of either DRG sections or DRG cultured neurons using the Fiji software. The integrated density was calculated as the sum of the values of the pixels in both cytoplasmic and nuclear regions of interest determined on the basis of TuJ-1, CGRP, TRPV1 or DAPI staining, respectively.

Analyses of transduction efficiency: AAV9 or AAV-PHP.S-driven transduction efficiency was determined using high-resolution confocal z-stack images from DRG and Spinal cord sections from animals injected with the appropriate AAV vector expressing GFP and either shCtrl or shα3. Images were converted to 8-bit, thresholds were defined, and the number of GFP/TuJ-1 double positive neurons counted using the ImageJ cell counter plugin. Cell numbers were expressed as percentage of GFP-positive neurons in the lumbar ventral horn and L4 DRGs.

Neuronal cultures

Adult mouse DRG neurons were cultured as previously described (*43*), with plating on poly-L-lysine and laminin coated plates or glass cover slips for 24 hours. Where required, L3-L5 DRG neurons from the uninjured side served as controls for cultures from SNI mice.

Proximity Ligation Assay (PLA) in DRG cultures

The Proximity Ligation Assay (PLA) is used to detect spatial proximity within ~40 nm of two proteins of interest (*46*). DRG neurons were cultured for 24 hours and fixed for 20 minutes in 4% PFA before blocking and permeabilization with 5% Donkey Serum, 1% BSA, 0.1% Triton X-100 in PBS for 1hr. They were then incubated with anti-c-Fos (mouse monocolonal 1:1000, Abcam ab208942) and anti-importin α3 (rabbit polyclonal, 1:2000, Michael Bader lab', MDC Berlin) overnight at 4˚C. PLA was performed using Duolink (Sigma: PLA probe anti-mouse minus DUO92004, anti-rabbit plus DUO92002 with detection using Far-Red DUO92013), according to the manufacturer's instructions. Identification of PLA signal within neurons was done by subsequent immunostaining with goat anti-CGRP

(AbD SEROTEC 1720-9007, IF 1:1000) for 60 min at room temperature, followed by three washes and an additional 60 min incubation with donkey anti-goat Alexa Fluor 488 (Jackson Immunoresearch, 1:1000). Cells were then washed, mounted with Flouromount-G™ (ThermoFisher Scientific, cat. # 00-4958-02) and imaged by confocal microscopy (Olympus FV1000, 60x oil-immersion objective Olympus UPLSAPO - NA 1.35). PLA signals were quantified by counting puncta in ImageJ.

Immunoblots from DRG neurons

Cultured DRG neurons were lysed directly in Laemmli buffer and analyzed by immunoblot using 5% BSA for blocking and overnight incubations with the following antibodies: anti-importin α3 1:5000 (rabbit polyclonal, Bader group, MDC Berlin), anti-c-Fos 1:1000 (mouse monoclonal, clone 2H2, Abcam ab208942), anti-TRPV1 (rabbit polyclonal, Alomone # ACC-030, 1:500). Blots were developed using Radiance ECL (Azure) or SuperSignal™ West Femto (Thermo Scientific) chemiluminescence substrates and quantified with Fiji.

Proximity biotinylation

Proximity biotinylation (*47*) was performed by transfecting fusion constructs with the miniTurbo enzyme (*48*) in N2a cells. Transfections were done with jetPEI™ (Polyplus-transfection), and labelling with 500 µM biotin was initiated 48 hours after transfection. Labeling was stopped after 6 hours by transferring the cells to ice and washing five times with ice-cold PBS. Lysis and streptavidin affinity purification were as previously described (*47*).

Transcriptome and gene expression analyses

Library Construction and Sequencing: Total RNA was extracted from adult DRGs (dorsal root ganglia) tissue, dissected from importin α3 KO and wild type male mice, using the RNAqueous-Micro Kit (Ambion). Replicates of high RNA integrity (RIN≥7) were processed for RNA-Seq at the Crown Institute for Genomics (G-INCPM, Weizmann Institute of Science).

500 ng of total RNA for each sample was processed using the in-house polyA-based RNA seq protocol (INCPM mRNA Seq). Libraries were evaluated by Qubit and TapeStation. Sequencing libraries were constructed with barcodes to allow multiplexing of 18 samples on two lanes of Illumina HiSeq machine, using the Single-Read 60 protocol (v4). The output

was ~27 million reads per sample. Fastq files for each sample were generated by the usage bcl2fastq-v2.17.1.14.

Sequence Data Analysis: Poly-A/T stretches and Illumina adapters were trimmed from the reads using cutadapt (*49*); and trimmed reads shorter than 30bp were discarded. Reads for each sample were aligned independently to the *Mus musculus* reference genome GRCm38 using STAR (2.4.2a) (*50*), supplied with gene annotations downloaded from Ensembl (and with EndToEnd option). The percentage of the reads that were aligned uniquely to the genome was ~78%. Counting proceeded over genes annotated in Ensemble release 92 using htseq-count (version 0.6.1p1) (*51*). Only uniquely mapped reads were used to determine the number of reads falling into each gene (intersection-strict mode). Differential analysis was performed using DESeq2 package (1.10.1) (*52*) with the betaPrior, cooksCutoff and independentFiltering parameters set to False. Raw P values were adjusted for multiple testing using the procedure of Benjamini and Hochberg. Differentially expressed genes, were determined by a p-adj of < 0.05, absolute fold changes > 1.5 and max raw counts > 30.

Data availability: The RNA-seq data generated from this paper have been deposited in NCBI's Gene Expression Omnibus (GEO) and are accessible through GEO series accession number GSE137515.

Transcription Factor Binding Site (TFBS) analysis: We assessed possible enrichment of different TFBS in datasets of regulated genes using FMatch (geneXplain) on gene sets with fold changes of two or more and their corresponding background sets. Promoter sequences from the importin α3 null dataset and a list of background genes (non-deregulated genes) were scanned from 600 base pairs (bp) upstream to 100 bp downstream of the predicted transcription start site for each gene, and TFBS were identified with the TRANSFAC FMatch tool. TFBS enrichment in test versus background sets was assessed by *t* test with p-value threshold of 0.05.

Gene expression analysis by RT-qPCR: Total RNA from DRG neuronal cultures and DRG tissue from SNI mice were extracted using the Ambion RNAqueous-Micro total RNA isolation kit (Life Technologies Corp.). RNA purity, integrity (RIN>8) and concentration was determined, and 100-200 ng of total RNA was then used to synthesize cDNA using SuperScript III (Invitrogen). RT-qPCR was performed on a ViiA7 System (Applied Biosystems) using PerfeCTa SYBR Green (Quanta Biosciences, Gaithersburg, USA). Forward/Reverse primers were designed for different exons, and the RNA was treated with DNase H to avoid false-positives. Amplicon specificity was verified by melting curve analysis. All RT-qPCR reactions were conducted in technical triplicates and the results were

averaged for each sample, normalized to *Actb* levels and the relevant reporter genes such as *GFP* and for the viruses, and analyzed using the comparative ΔΔCt method (*53*). The following primers (*Mus musculus*) were used:
Actb (F: GGCTGTATTCCCCTCCATCG – R: CCAGTTGGTAACAATGCCATGT),
Kpna4/importinα3 (F: CCAGTGATCGAAATCCACCAA, R: CGTTTGTTCAGACGTTCCAGAT),
GFP (F: ACGTAAACGGCCACAAGTTC - R: GTGTACTTCGTCGTGCTGAA),
Syngap1 (F: GGGACAAATGGATTGAGAATCTG- R: GGCGGCTGTTGTCCTTGTT),
Slc38a1 (F:ACTTCCTGACGGCCATCTTT-R: GTCGCCTGTGCTCTGGTACT),
Gpr151 (F: GCATGCTTCGCGTATGCA – R: GATGGTGCGGCTGTGGATA),
Rtl1 (F: CCGCTTTCGGTATCACAACA- R: CGGTCTGGCGATGGAACT).

Viral constructs – cloning, AAV production and validation

AAV shRNA constructs were based on AAV-shRNA-ctrl (Addgene plasmid #85741, U6 promoter) with specific shRNA sequences cloned in using BamHI and XbaI restriction sites. The target sequence (with overhangs) selected for importin α3 was GATCCGGCTTTGACAAACATTGCATGAAGCTTGATGCAATGTTTGTCAAAGCCTTTTTT. Sequences of additional targets used were as follows:
shFos 1 -
GATCCGGCGGAGACAGATCAACTTGAAGAAGCTTGTTCAAGTTGATCTGTCTCCGCCTTTTTTT
shFos 2 -
GATCCGGGACCTTACCTGTTCGTGAAACGAAGCTTGGTTTCACGAACAGGTAAGGTCCCTTTTTTT
shJun -
GATCCGGCACATCACCACTACACCGACCCCCACCCGAAGCTTGGGGTGGGGGTCGGTGTAGTGGTGATGTGCCTTTTTTT

For overexpression experiments, an AAV backbone was generated, driving expression from a human Synapsin I (hSynI) promoter to ensure neuronal specificity (*54*). The AAV backbone was modified by inserting a multiple cloning site between hSyn and WPRE, which was then used to introduce the following inserts:
1) A dominant negative A-Fos sequence (*30*) obtained from Addgene (plasmid #33353) was amplified with added restriction sites for AscI and EcoRV, and inserted into the AAV backbone, generating pAAV-hSyn-A-Fos-WPRE.

2) The mouse importin α3 ORF was amplified from mouse brain cDNA using Phusion DNA polymerase and cloned into the AAV backbone specified above to generate pAAV-hSyn-Importin α3-WPRE.
3) Control constructs contained an EGFP insert, designated pAAV-hSyn-EGFP-WPRE.

Transfection and immunoblot analysis: Knockdown and overexpression constructs were tested in HEK or N2A cells, transfected using JetPEI™ (Polyplus-transfection) according to manufacturer's instructions and lysed 48h later in RIPA buffer supplemented with protease inhibitors (Complete, Roche). For immunoblot analysis, 5 µg of protein was separated on TGX Protean 5-15% gradient gels (Biorad) and transferred to nitrocellulose membranes. Membranes were blocked with 5% dried milk-TBST and probed overnight with importin α3 antibody (1:5000, Michael Bader lab', MDC Berlin) and GAPDH (1:5000, MAB374, Millipore) as loading control in 2% milk-TBST, followed by anti-mouse HRP-conjugated antibodies (#1706516 Biorad). Chemiluminescence was detected with Amersham Imager 600 and band intensities were quantified using the built-in software.

AAV generation and intrathecal injection

We used AAV serotype 9 (AAV9) or the peripheral neuron specific PHP.S (AAV-PHP.S) (*21*) for knockdown or overexpression experiments. Both serotypes were produced in HEK 293T cells (ATCC®), with the AAVpro® Purification Kit (All Serotypes) from TaKaRa (#6666). For each construct ten 15 cm plates were transfected with 20 µg of DNA (AAV-plasmid containing the construct of interest and two AAV9 or AAV-PHP.S helper plasmids) using jetPEI™ (Polyplus-transfection) in DMEM medium without serum or antibiotics. pAAV2/9n and pAdDeltaF6 helper vectors were obtained from the University of Pennsylvania Vector Core, pPHP.S helper plasmid was obtained from Addgene (plasmid #103006). Medium (DMEM, 20 % FBS, 1 mM sodium pyruvate, 100 U/mL penicillin 100 mg/mL streptomycin) was added on the following day to a final concentration of 10% FBS and extraction was done at three days post transfection. Purification was performed according to the manufacturer's instructions. For all constructs, we obtained titers in the range of 10^{12}-10^{13} viral genomes/ml, which were used undiluted for intrathecal injections into the lumbar segments of the spinal cord (5 µl/animal).

Statistical Analyses

All data underwent normality testing using the Shapiro-Wilk test. Potential outliers were discarded using the ROUT method with a Q (maximum desired false discovery rate) of 1%. Datasets that passed the normality test were subjected to parametric analysis. Unpaired Student's t-test was used for analyses with two groups, one-way ANOVA was used to compare multiple groups, two-way ANOVA was used to compare mice over time. In the follow-up analyses all experimental conditions were compared to one control condition using Tukey's or Dunnett's multiple comparisons tests. Datasets that did not pass the normality test were subjected to nonparametric analysis using the Kruskal-Wallis test on rank for multiple group statistical evaluation followed by Dunn's multiple comparisons test. For 2-groups analyses, the Mann-Whitney test was used. The results are expressed throughout as mean ± standard error of the mean (SEM). All analyses were performed using GraphPad Prism version 7.00 for Windows (GraphPad Software, La Jolla, California, USA, www.graphpad.com). Statistically significant *p* values are shown as * $p < 0.05$, ** $p < 0.01$, *** $p < 0.001$ and **** $p < 0.0001$. All statistical parameters for specific analyses are detailed in the corresponding figure legends.

References cited

1. Y. Miyamoto, K. Yamada, Y. Yoneda, Importin alpha: a key molecule in nuclear transport and non-transport functions. *J Biochem* **160**, 69-75 (2016).
2. M. Christie *et al.*, Structural Biology and Regulation of Protein Import into the Nucleus. *J Mol Biol* **428**, 2060-2090 (2016).
3. N. Panayotis, A. Karpova, M. R. Kreutz, M. Fainzilber, Macromolecular transport in synapse to nucleus communication. *Trends Neurosci* **38**, 108-116 (2015).
4. M. Terenzio, G. Schiavo, M. Fainzilber, Compartmentalized signaling in neurons: from cell biology to neuroscience. *Neuron* **96**, 667-679 (2017).
5. B. Friedrich, C. Quensel, T. Sommer, E. Hartmann, M. Kohler, Nuclear localization signal and protein context both mediate importin alpha specificity of nuclear import substrates. *Mol Cell Biol* **26**, 8697-8709 (2006).
6. M. T. Mackmull *et al.*, Landscape of nuclear transport receptor cargo specificity. *Mol Syst Biol* **13**, 962 (2017).
7. T. Shmidt *et al.*, Normal brain development in importin-alpha5 deficient-mice. *Nat Cell Biol* **9**, 1337-1338; author reply 1339 (2007).
8. F. Rother *et al.*, Importin alpha7 is essential for zygotic genome activation and early mouse development. *PLoS One* **6**, e18310 (2011).

9. G. Gabriel *et al.*, Differential use of importin-alpha isoforms governs cell tropism and host adaptation of influenza virus. *Nat Commun* **2**, 156 (2011).
10. T. Moriyama *et al.*, Targeted disruption of one of the importin alpha family members leads to female functional incompetence in delivery. *FEBS J* **278**, 1561-1572 (2011).
11. K. Ben-Yaakov *et al.*, Axonal transcription factors signal retrogradely in lesioned peripheral nerve. *The EMBO journal* **31**, 1350-1363 (2012).
12. N. Yasuhara *et al.*, Importin alpha subtypes determine differential transcription factor localization in embryonic stem cells maintenance. *Dev Cell* **26**, 123-135 (2013).
13. N. Panayotis *et al.*, Importin alpha5 Regulates Anxiety through MeCP2 and Sphingosine Kinase 1. *Cell Rep* **25**, 3169-3179 (2018).
14. A. S. Sowa *et al.*, Karyopherin alpha-3 is a key protein in the pathogenesis of spinocerebellar ataxia type 3 controlling the nuclear localization of ataxin-3. *Proc Natl Acad Sci U S A* **115**, E2624-E2633 (2018).
15. K. Dohner *et al.*, Importin alpha1 is required for nuclear import of herpes simplex virus proteins and capsid assembly in fibroblasts and neurons. *PLoS Pathog* **14**, e1006823 (2018).
16. I. Decosterd, C. J. Woolf, Spared nerve injury: an animal model of persistent peripheral neuropathic pain. *Pain* **87**, 149-158 (2000).
17. M. Pertin, R. D. Gosselin, I. Decosterd, The spared nerve injury model of neuropathic pain. *Methods Mol Biol* **851**, 205-212 (2012).
18. S. Shiers *et al.*, Neuropathic Pain Creates an Enduring Prefrontal Cortex Dysfunction Corrected by the Type II Diabetic Drug Metformin But Not by Gabapentin. *J Neurosci* **38**, 7337-7350 (2018).
19. H. Abdo *et al.*, Specialized cutaneous Schwann cells initiate pain sensation. *Science* **365**, 695-699 (2019).
20. X. Yu *et al.*, Dorsal root ganglion macrophages contribute to both the initiation and persistence of neuropathic pain. *Nature Communications* **11**, 264 (2020).
21. K. Y. Chan *et al.*, Engineered AAVs for efficient noninvasive gene delivery to the central and peripheral nervous systems. *Nat Neurosci* **20**, 1172-1179 (2017).
22. R. E. Coggeshall, Fos, nociception and the dorsal horn. *Prog Neurobiol* **77**, 299-352 (2005).
23. P. L. Santos, R. G. Brito, J. Matos, J. S. S. Quintans, L. J. Quintans-Junior, Fos Protein as a Marker of Neuronal Activity: a Useful Tool in the Study of the Mechanism of Action of Natural Products with Analgesic Activity. *Mol Neurobiol* **55**, 4560-4579 (2018).
24. J. Lai *et al.*, Dynorphin A activates bradykinin receptors to maintain neuropathic pain. *Nat Neurosci* **9**, 1534-1540 (2006).

25. S. D. Michaelson *et al.*, SYNGAP1 heterozygosity disrupts sensory processing by reducing touch-related activity within somatosensory cortex circuits. *Nature Neuroscience* **21**, 1-13 (2018).
26. M. Arnold, A. Nath, D. Wohlwend, R. H. Kehlenbach, Transportin is a major nuclear import receptor for c-Fos: a novel mode of cargo interaction. *J Biol Chem* **281**, 5492-5499 (2006).
27. N. Sharma *et al.*, The emergence of transcriptional identity in somatosensory neurons. *Nature* **577**, 392-398 (2020).
28. Y. Aikawa *et al.*, Treatment of arthritis with a selective inhibitor of c-Fos/activator protein-1. *Nat Biotechnol* **26**, 817-823 (2008).
29. H. Makino *et al.*, A selective inhibition of c-Fos/activator protein-1 as a potential therapeutic target for intervertebral disc degeneration and associated pain. *Sci Rep* **7**, 16983 (2017).
30. M. Olive *et al.*, A dominant negative to activation protein-1 (AP1) that abolishes DNA binding and inhibits oncogenesis. *J Biol Chem* **272**, 18586-18594 (1997).
31. J. Lamb *et al.*, The Connectivity Map: using gene-expression signatures to connect small molecules, genes, and disease. *Science* **313**, 1929-1935 (2006).
32. A. J. Mears *et al.*, Mining the transcriptome for rare disease therapies: a comparison of the efficiencies of two data mining approaches and a targeted cell-based drug screen. *NPJ Genom Med* **2**, 14 (2017).
33. T. Huang *et al.*, Identifying the pathways required for coping behaviours associated with sustained pain. *Nature* **565**, 86-90 (2019).
34. P. Ray *et al.*, Comparative transcriptome profiling of the human and mouse dorsal root ganglia: an RNA-seq-based resource for pain and sensory neuroscience research. *Pain* **159**, 1325-1345 (2018).
35. R. Y. North *et al.*, Electrophysiological and transcriptomic correlates of neuropathic pain in human dorsal root ganglion neurons. *Brain* **142**, 1215-1226 (2019).
36. A. S. Yekkirala, D. P. Roberson, B. P. Bean, C. J. Woolf, Breaking barriers to novel analgesic drug development. *Nat Rev Drug Discov* **16**, 545-564 (2017).
37. T. J. Price *et al.*, Transition to chronic pain: opportunities for novel therapeutics. *Nat Rev Neurosci* **19**, 383-384 (2018).
38. P. Skolnick, N. D. Volkow, Re-energizing the Development of Pain Therapeutics in Light of the Opioid Epidemic. *Neuron* **92**, 294-297 (2016).
39. L. Urien *et al.*, Genetic ablation of GINIP-expressing primary sensory neurons strongly impairs Formalin-evoked pain. *Sci Rep* **7**, 43493 (2017).

40. J. P. Golden *et al.*, RET signaling is required for survival and normal function of nonpeptidergic nociceptors. *J Neurosci* **30**, 3983-3994 (2010).
41. S. Nakamori *et al.*, Ephedra Herb extract activates/desensitizes transient receptor potential vanilloid 1 and reduces capsaicin-induced pain. *J Nat Med* **71**, 105-113 (2017).
42. L. Marvaldi *et al.*, Enhanced axon outgrowth and improved long-distance axon regeneration in sprouty2 deficient mice. *Dev Neurobiol* **75**, 217-231 (2015).
43. R. B. Perry *et al.*, Subcellular knockout of importin beta1 perturbs axonal retrograde signaling. *Neuron* **75**, 294-305 (2012).
44. J. N. Crawley, Behavioral phenotyping strategies for mutant mice. *Neuron* **57**, 809-818 (2008).
45. S. Y. Dagan, M. M. Tsoory, M. Fainzilber, N. Panayotis, COLORcation: A new application to phenotype exploratory behavior models of anxiety in mice. *J Neurosci Methods* **270**, 9-16 (2016).
46. O. Söderberg *et al.*, Direct observation of individual endogenous protein complexes in situ by proximity ligation. *Nature Methods* **3**, 995-1000 (2006).
47. K. J. Roux, D. I. Kim, M. Raida, B. Burke, A promiscuous biotin ligase fusion protein identifies proximal and interacting proteins in mammalian cells. *Journal of Cell Biology* **196**, 801-810 (2012).
48. T. C. Branon *et al.*, Efficient proximity labeling in living cells and organisms with TurboID. *Nat Biotechnol* **36**, 880-887 (2018).
49. M. Martin, Cutadapt removes adapter sequences from high-throughput sequencing reads. *EMBnet.journal* **17**, 10-12 (2011).
50. A. Dobin *et al.*, STAR: ultrafast universal RNA-seq aligner. *Bioinformatics* **29**, 15-21 (2013).
51. S. Anders, P. T. Pyl, W. Huber, HTSeq--a Python framework to work with high-throughput sequencing data. *Bioinformatics* **31**, 166-169 (2014).
52. M. I. Love, W. Huber, S. Anders, Moderated estimation of fold change and dispersion for RNA-seq data with DESeq2. *Genome Biology* **15**, 550 (2014).
53. K. J. Livak, T. D. Schmittgen, Analysis of relative gene expression data using real-time quantitative PCR and the 2(-Delta Delta C(T)) Method. *Methods* **25**, 402-408 (2001).
54. M. Mahn *et al.*, High-efficiency optogenetic silencing with soma-targeted anion-conducting channelrhodopsins. *Nat Commun* **9**, 4125 (2018).

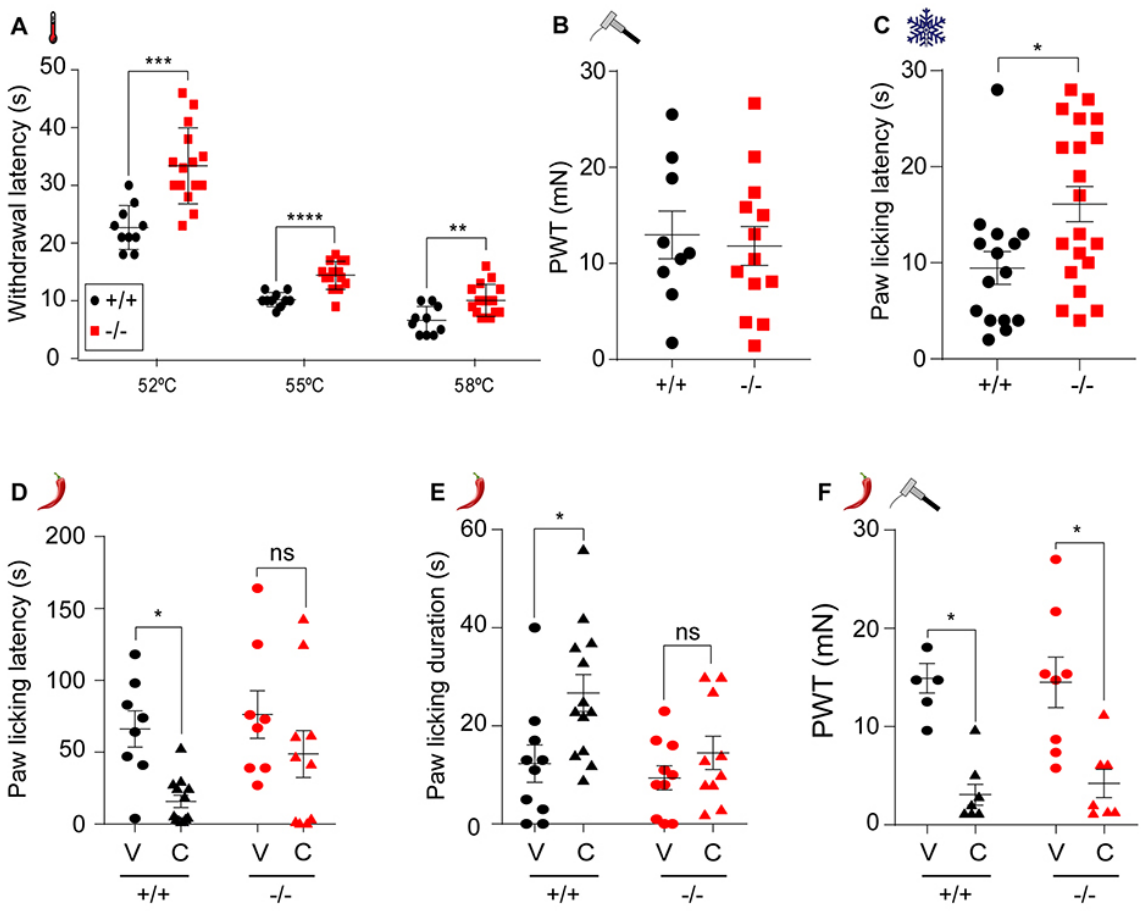

Fig. S1. Reduced sensitivity to noxious stimuli in importin α3 mice. (**A**) Hot plate assays at 52, 55 and 58ºC reveal reduced heat sensitivity in importin α3 knockout mice. n ≥ 10, ** indicates $p < 0.005$, *** indicates $p < 0.001$; **** indicates $p < 0.0001$, ANOVA followed by Tukey's multiple comparison test. (**B**) No differences in basal mechanosensitivity measured as paw withdrawal threshold (PWT) in the von Frey test in importin α3 null versus wild type mice. n ≥ 9. (**C**) Acetone tests show somewhat reduced cold sensitivity in importin α3 null mice. n ≥ 15, * indicates $p < 0.05$, two-tailed unpaired *t*-test. (**D**, **E**) Lower sensitivity in spontaneous response to capsaicin in importin α3 null mice. n ≥ 8, Kruskal-Wallis test followed by Dunn's multiple comparison test, * indicates $p < 0.05$. (**F**) No differences in mechanosensitivity between importin α3 null and wild type mice as measured by PWT in the von Frey test one hour after injection of capsaicin. n ≥ 5, Kruskal-Wallis test followed by Dunn's multiple comparison test, * indicates $p < 0.05$. All data are shown as mean ± SEM.

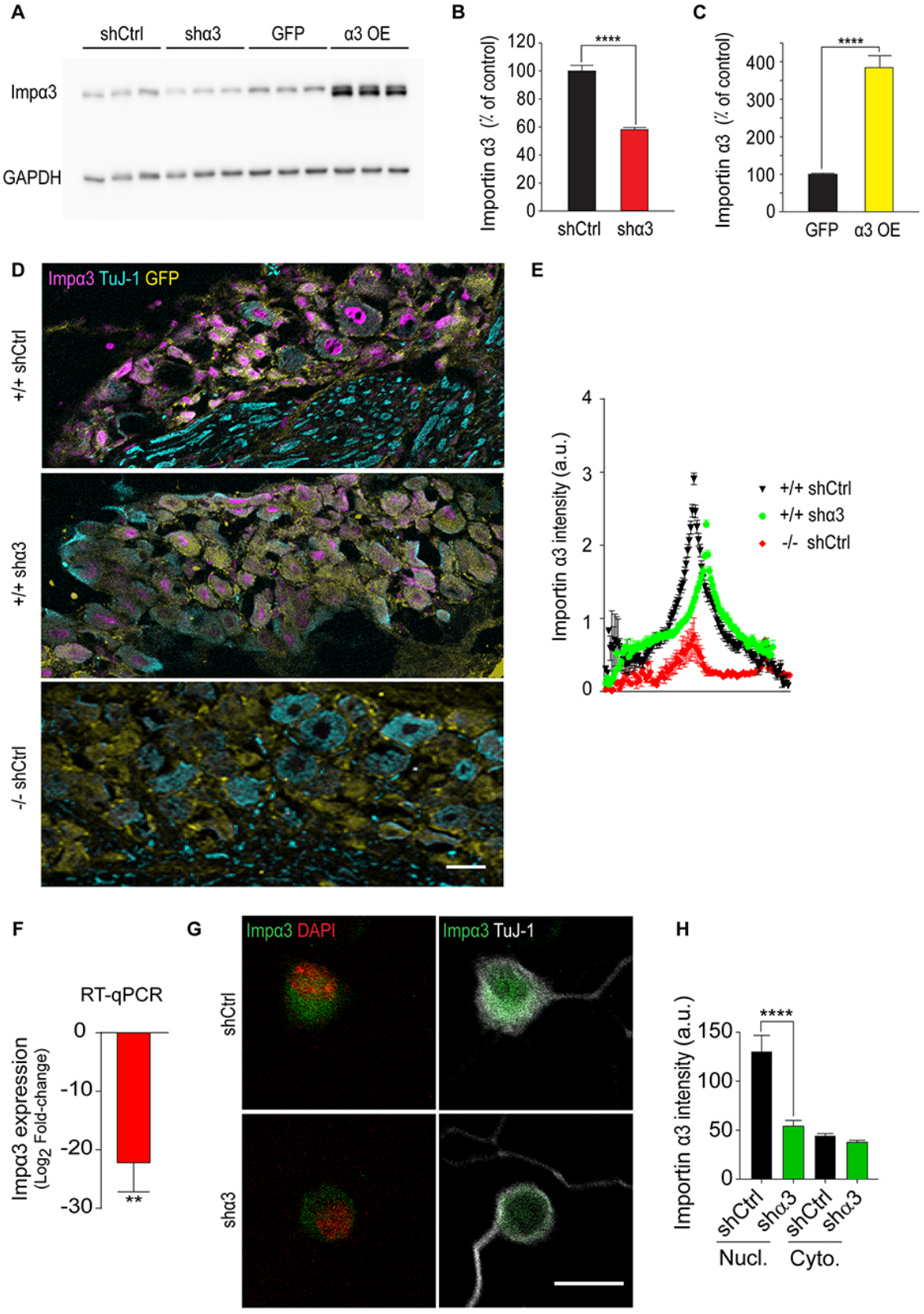
A
shCtrl
shα3
GFP
α3 OE
Impα3
GAPDH
B
Importin α3 (% of control)
120
100
80
60
40
20
0
****
shCtrl
shα3
C
Importin α3 (% of control)
400
300
200
100
0
****
GFP
α3 OE
D
Impα3 TuJ-1 GFP
+/+ shCtrl
+/+ shα3
-/- shCtrl
E
Importin α3 intensity (a.u.)
4
3
2
1
0
+/+ shCtrl
+/+ shα3
-/- shCtrl
F
RT-qPCR
Impα3 expression
(Log2 Fold-change)
0
-10
-20
-30
**
G
Impα3 DAPI
Impα3 TuJ-1
shCtrl
shα3
H
Importin α3 intensity (a.u.)
150
100
50
0
****
shCtrl
shα3
shCtrl
shα3
Nucl.
Cyto.

Fig. S2. Validation of AAV9 vectors for knockdown or overexpression of importin α3. (A) Immunoblot analyses of importin α3 in protein extracts from N2a cells transduced with AAV9 expressing shCtrl or shα3 for knockdown, or eGFP or importin α3 for overexpression (OE). (**B, C**) Quantification of importin α3 protein levels from A shows significant downregulation in shα3-treated cells compared to shCtrl (B), and upregulation in α3-OE cells compared to GFP (C). GAPDH served for normalization in both cases. n=3, **** indicates p <0.0001, unpaired two-tailed t-test. (**D**) Immunostaining of DRG sections from wild-type (+/+) or importin α3 null (-/-) mice one month after intrathecal injection with AAV9 vectors expressing eGFP and the indicated shRNA. Scale bar 40 μm. (**E**) Line scan intensity measurements reveal a reduction of importin α3 signal in shα3-treated wild type animals compared to shCtrl (+/+ shCtrl, n=210; +/+ shα3, n=204 and -/- shCtrl, n=5 neurons). (**F**) RT-qPCR quantification of importin α3 expression in mouse DRG cultures one month after intrathecal injection of viral constructs shows a significant downregulation of importin α3 mRNA in shα3-treated animals compared to shCtrl. n=3, ** indicates p <0.01, Unpaired two-tailed t-test. (**G**) DRG neurons from the cultures described in F immunostained for importin α3 and TuJ-1. Scale bar 15 μm. (**H**) Quantification of importin α3 immunofluorescence from the experiment shown in G revealed a significant reduction in nuclear levels in shα3-treated neurons. n ≥ 36 neurons, **** indicates p <0.0001, Unpaired two-tailed t-test. All data shown as mean ± SEM.

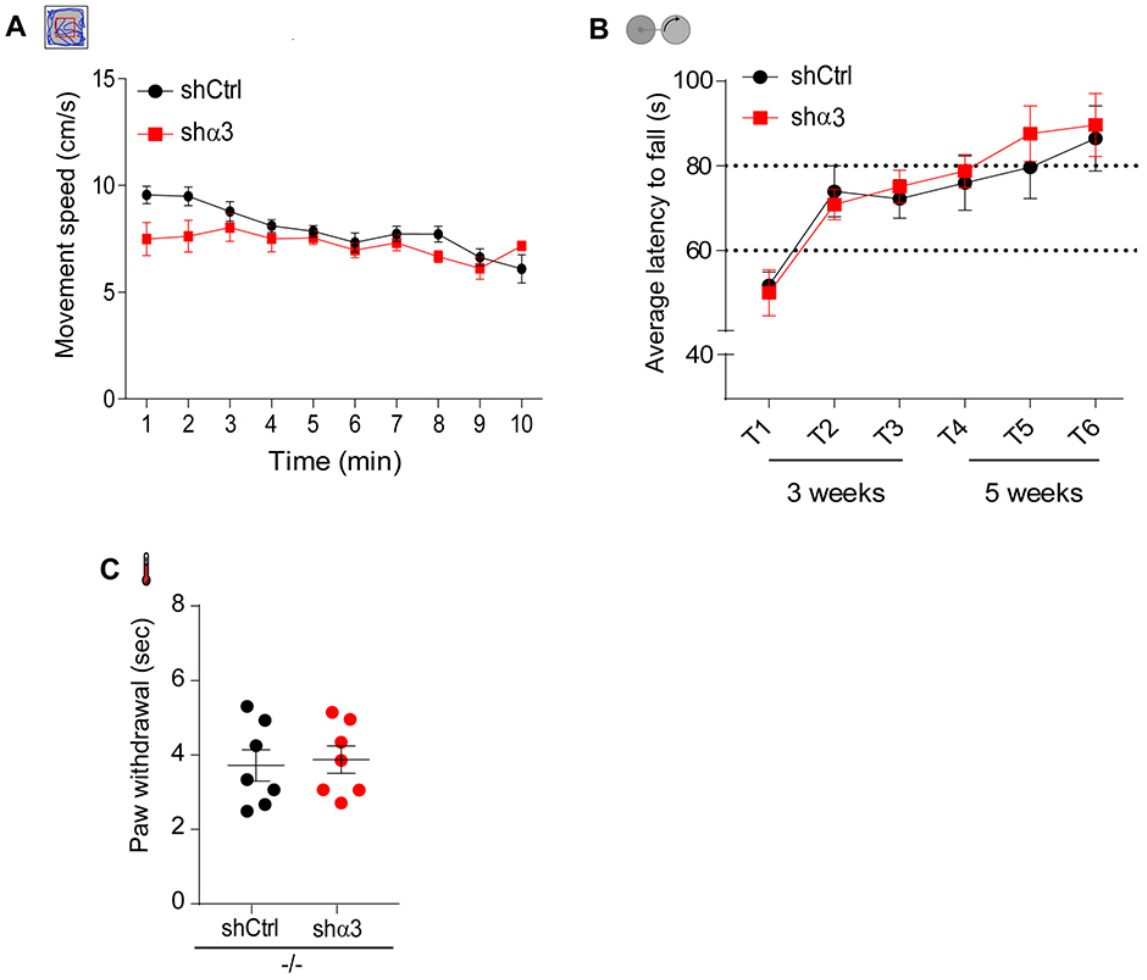

Fig. S3. AAV9-shRNA effects. No differences were observed in movement speed in open field (**A**) or in rotarod performance (**B**) in mice injected intrathecally with AAV9 expressing either control (shCtrl) or importin α3-targeting (shα3) shRNAs. (**C**) No additional effect of shCtrl or shα3-mediated knockdown on the reaction to noxious heat (tested using the heat probe test) in importin α3 knockout mice. All tests carried out 3-4 weeks after injection. n ≥ 7 per group. All data shown as mean ± SEM.

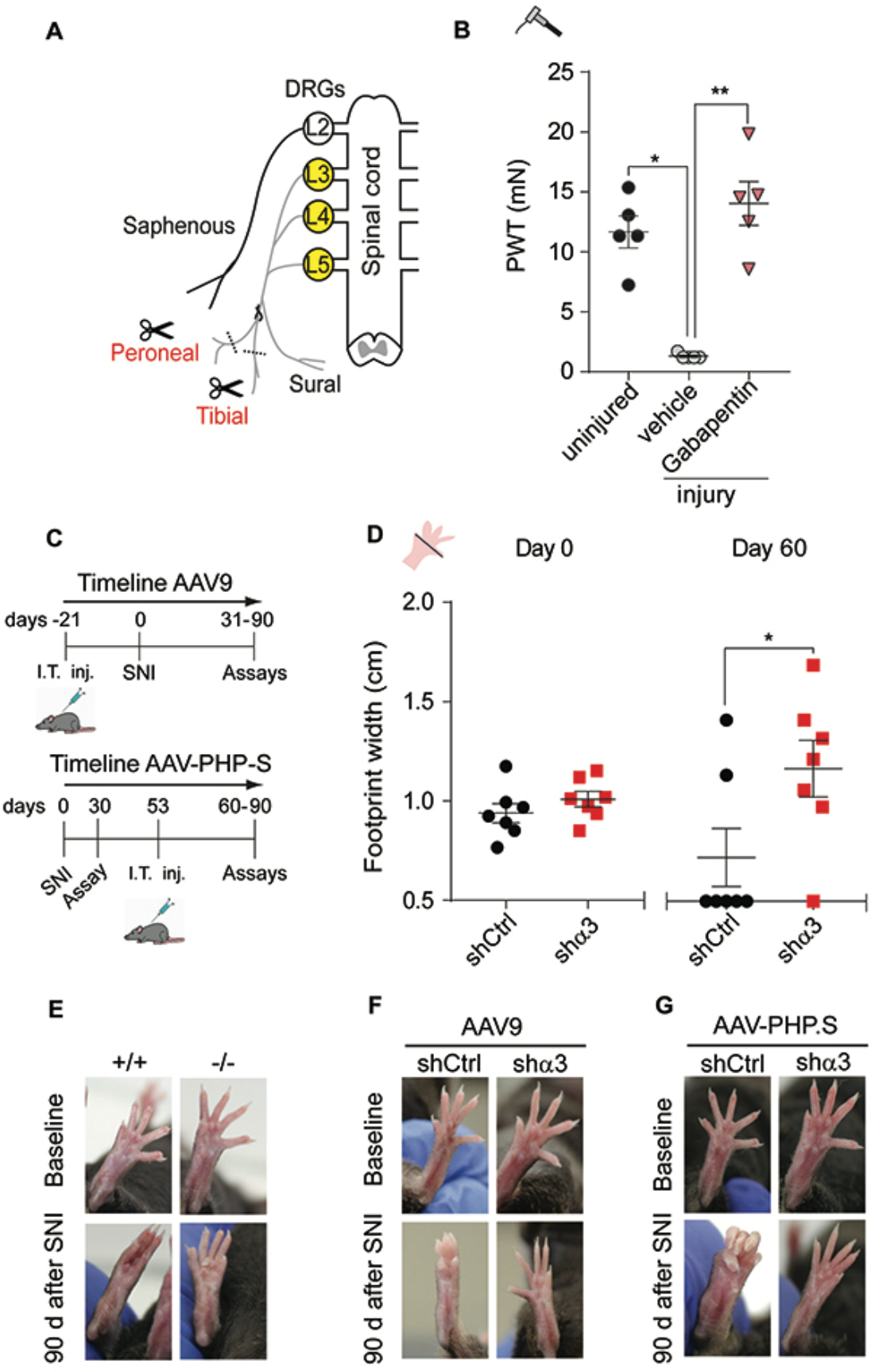
A
DRGs
L2
L3
L4
L5
Spinal cord
Saphenous
Peroneal
Sural
Tibial
B
PWT (mN)
25
20
15
10
5
0
*
**
uninjured
vehicle
Gabapentin
injury
C
Timeline AAV9
days -21
0
31-90
I.T. inj.
SNI
Assays
Timeline AAV-PHP-S
days 0
30
53
60-90
SNI
Assay
I.T. inj.
Assays
D
Day 0
Day 60
Footprint width (cm)
2.0
1.5
1.0
0.5
*
shCtrl
shα3
shCtrl
shα3
E
+/+
-/-
Baseline
90 d after SNI
F
AAV9
shCtrl
shα3
Baseline
90 d after SNI
G
AAV-PHP.S
shCtrl
shα3
Baseline
90 d after SNI

Fig. S4. Spared nerve injury (SNI) model. (**A**) Schematic of the spared nerve injury model (SNI). (**B**) Validation of the SNI model using gabapentin (100 mg/kg). Drug or vehicle (5% DMSO in PBS) were injected two months after establishing SNI and paw withdrawal threshold (PWT) was assessed by von Frey test. n = 5, * indicates $p < 0.05$, ** indicates $p < 0.01$, Kruskal-Wallis followed by Dunn's multiple comparison tests. (**C**) Paw images from SNI animals reveal recovery of paw morphology and reduced clenching in importin α3 knockout versus wild type animals. (**D**) Schematic showing timeline for shRNA-mediated knockdown by intrathecal injection of AAV9 or AAV-PHP.S in SNI. (**E**) Catwalk analyses of footprint width at two months after establishing SNI show a recovery in AAV9-shα3-treated animals. n = 7, * indicates $p < 0.05$, two-tailed unpaired *t*-test. All data shown as mean ± SEM. (**F**, **G**) Paw images from SNI animals reveal recovery of paw morphology and reduced clenching in importin α3 knockdown versus control shRNA treated animals. Data from AAV9 shRNA animals in F and from AAV-PHP.S shRNA animals in G. All data shown as mean ± SEM.

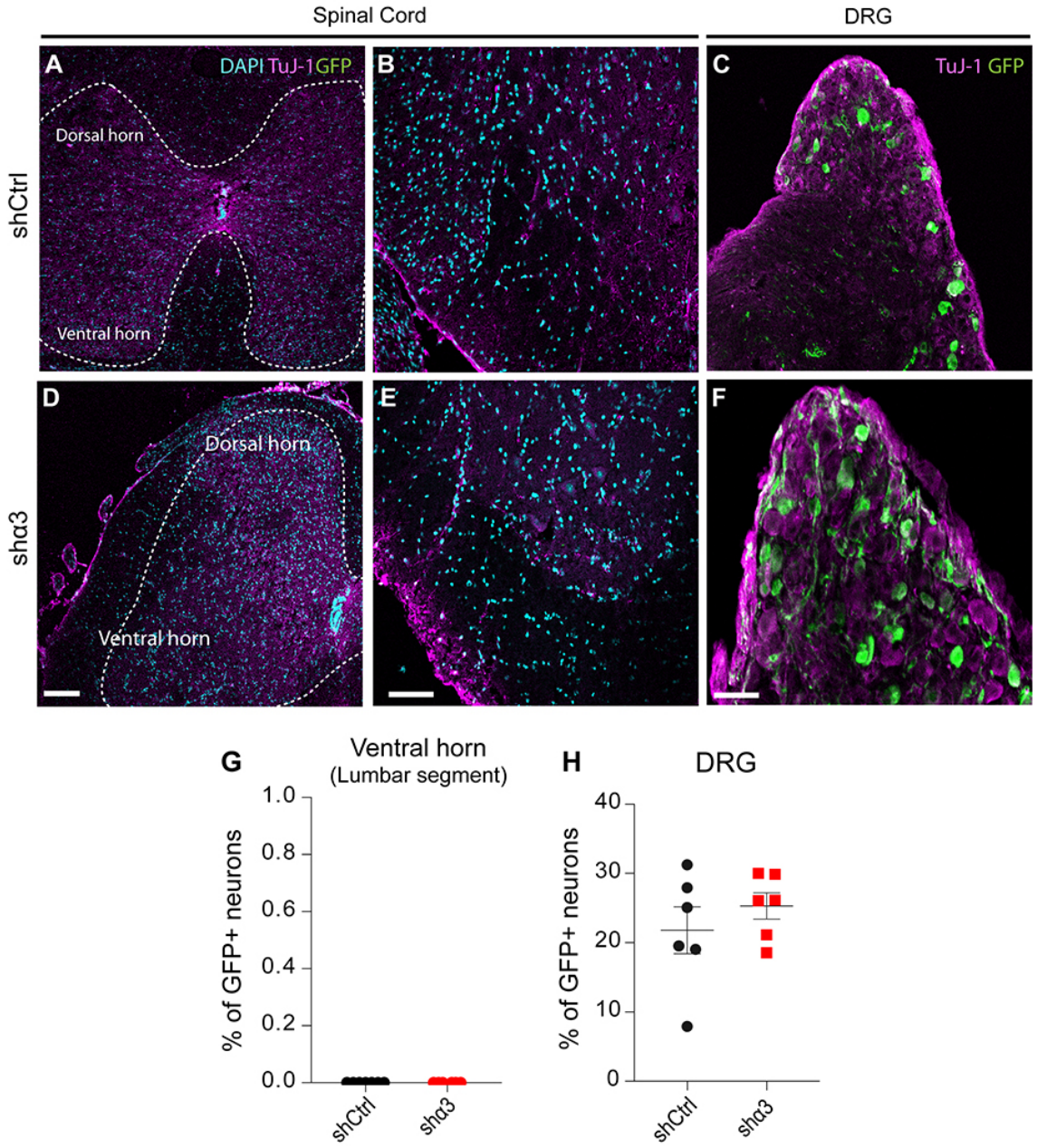

Fig. S5. Validation of peripheral neuron specificity of AAV-PHP.S viral constructs. Immunostaining for TuJ1 and GFP from spinal cord (lumbar section) and DRG of mice 6 weeks after intrathecal injection with AAV-PHP.S expressing GFP and either shCtrl (**A-C**) or shα3 (**D-F**). Panels **B** and **E** are enlargements from the ventral horn area in Panels **A** and **D**, respectively. Scale bars, D 150 µm, E, F 100 µm. (**G, H**) Percentage of GFP-positive neurons in the lumbar ventral horn (**G**) and L4 DRGs (**H**). n ≥ 6 per group. All data shown as mean ± SEM.

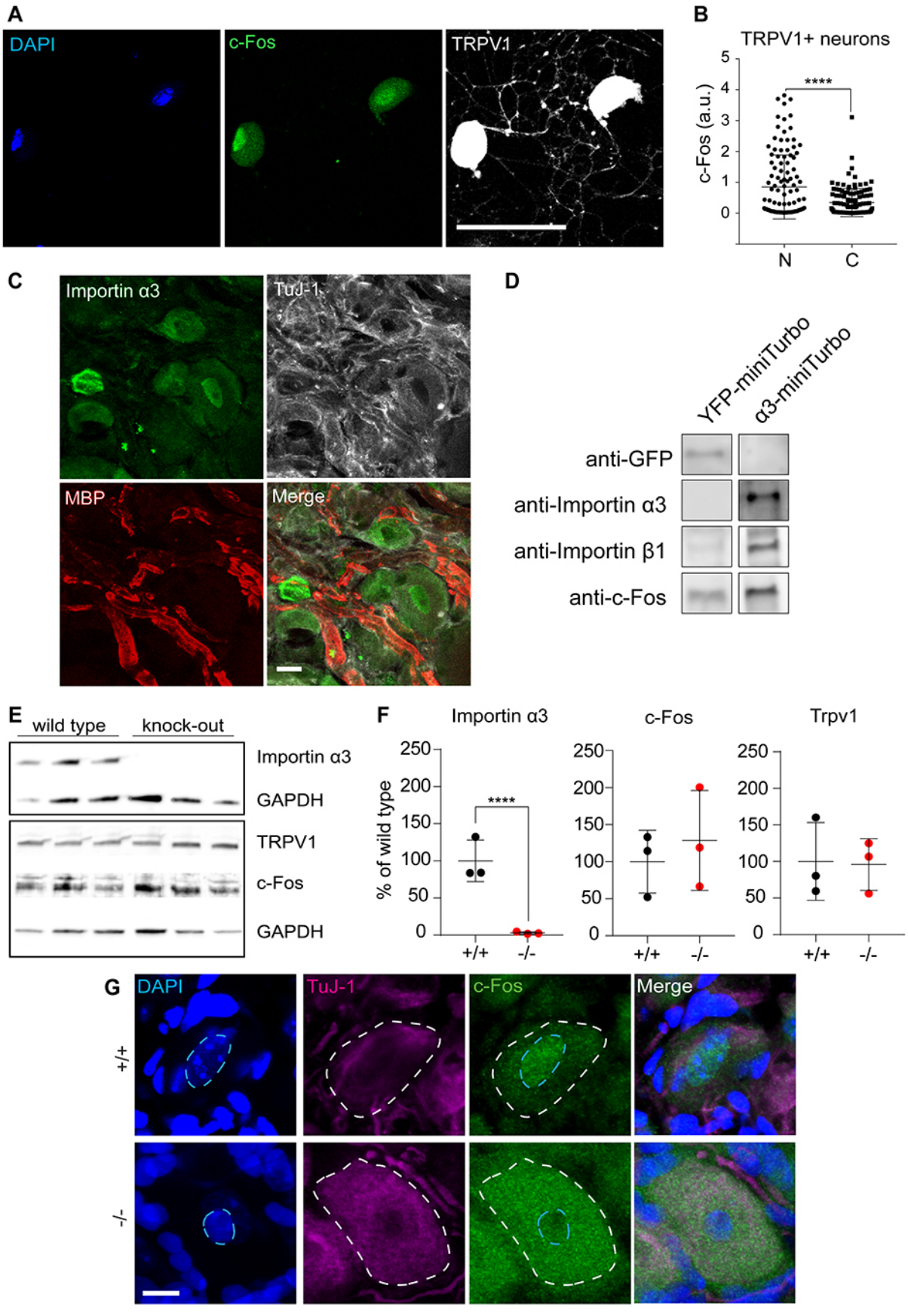
A
DAPI
c-Fos
TRPV1
B
TRPV1+ neurons
c-Fos (a.u.)
****
N
C
C
Importin α3
TuJ-1
MBP
Merge
D
YFP-miniTurbo
α3-miniTurbo
anti-GFP
anti-Importin α3
anti-Importin β1
anti-c-Fos
E
wild type
knock-out
Importin α3
GAPDH
TRPV1
c-Fos
GAPDH
F
Importin α3
c-Fos
Trpv1
% of wild type
****
+/+
-/-
G
DAPI
TuJ-1
c-Fos
Merge
+/+
-/-

Fig. S6. c-Fos expression and interaction with Importin α3. (**A**) DRG neurons harvested from ganglia 4 hr after SNI and cultured for 24 hr before immunostaining for c-Fos, TRPV1 and DAPI. Scale bar 100 μm. (**B**) Quantification of c-FOS in nucleus and cytoplasmic compartments of TRPV1-positive neurons from the cultures shown in A. n = 117, **** indicates $p < 0.0001$, Unpaired two-tailed *t*-test. (**C**) L4 DRG section immunostained for importin α3, TuJ-1 and MBP. Scale bar 10 μm. (**D**) N2a cells were transfected with BioID fusion proteins, YFP-miniTurbo and importin α3-miniTurbo. Biotinylated proteins were affinity purified after 6 hours incubation of the cultures with 500μM biotin and subjected to immunoblotting. Blots were probed for c-Fos, importin α3, and importin β1. (**E**) DRG neurons from wild type (+/+) and importin α3 knockouts (-/-) were cultured for 24 hours prior to immunoblot analyses as shown. (**F**) Quantification of the blots shown in E, normalized to GAPDH protein levels. n=3, data normalized to wild-type control. **** indicates $p < 0.0001$, one-tail *t*-test**.** (**G**) Reduced nuclear localization of c-Fos in DRG neurons from sectioned ganglia of importin α3 null compared to wild type mice. Immunostaining for TuJ-1, DAPI, c-Fos. Scale bar 10 μm. All quantitative data shown as mean ± SEM.

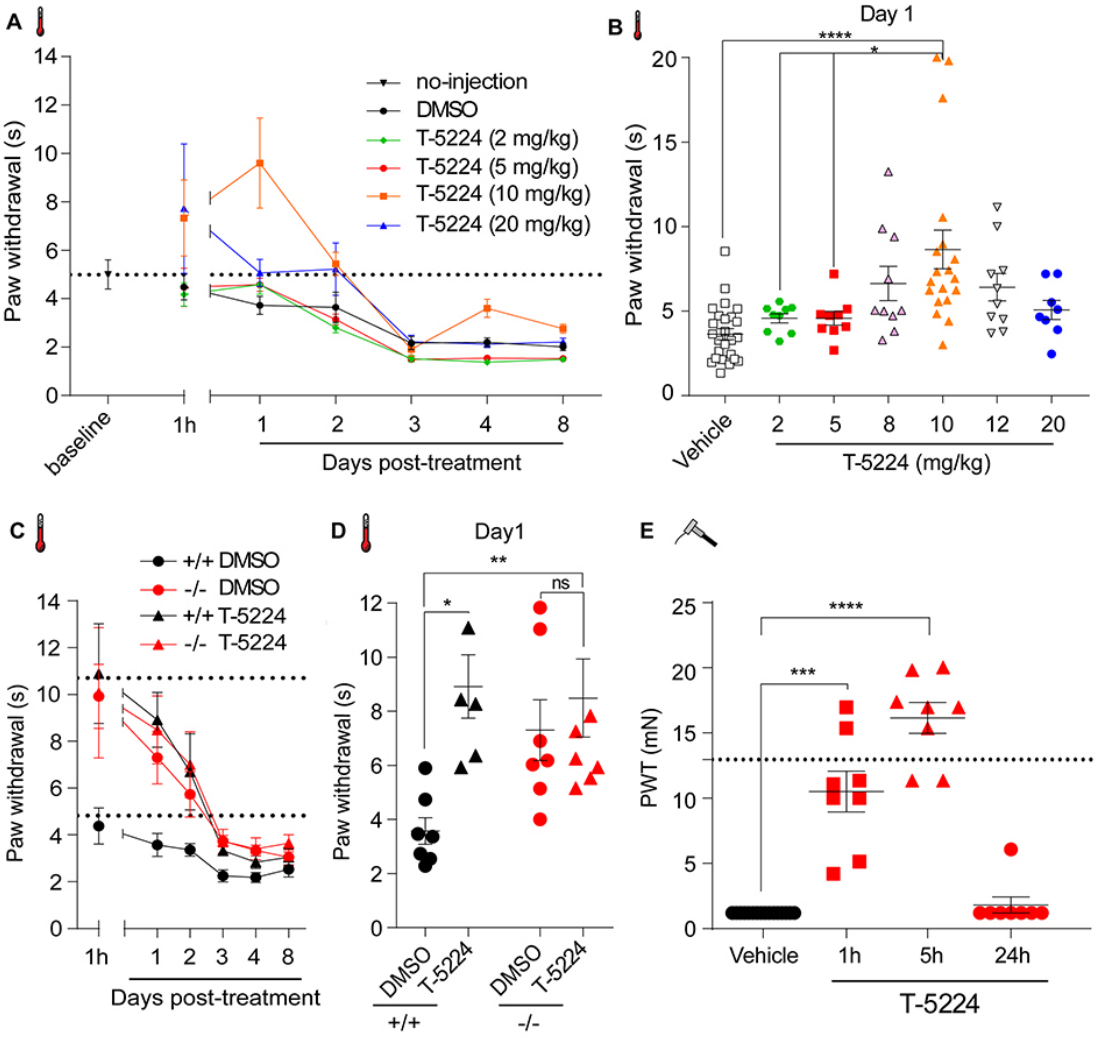

Fig. S7. Effects of the c-Fos inhibitor T-5224 on acute and chronic pain responses. (**A**) Effects of T-5224 on the response to noxious heat in wild-type mice. The drug was evaluated at the indicated dosages using the 58ºC heat probe test 1 hour after injection on day 1 and subsequently 2, 3, 4 and 8 days after treatment. (**B**) Additional dose-response analyses of T-5224 effects on the reaction to noxious heat one day after injection. For both panels n ≥ 8, * indicates $p < 0.05$, **** indicates $p < 0.0001$, ANOVA followed by Tukey's multiple comparison test. (**C**) T-5224 (10 mg/kg, i.p.) reduces the response to noxious heat in wild type mice over eight consecutive days of assay, but has no additional effect in importin α3 null mice. (**D**) The average paw withdrawal latency at one day after treatment in the experiment detailed in C. n ≥ 5, * indicates $p < 0.05$, ** indicates $p < 0.01$, ANOVA followed by Tukey's multiple comparison tests. (**E**) PWT in animals treated with 10 mg/kg T-5224 one week after SNI, and assessed by the von Frey test at the indicated times after treatment. n = 8, *** indicates $p < 0.001$, **** indicates $p < 0.0001$. Kruskal-Wallis followed by Dunn's multiple comparison tests. All data shown as mean ± SEM.

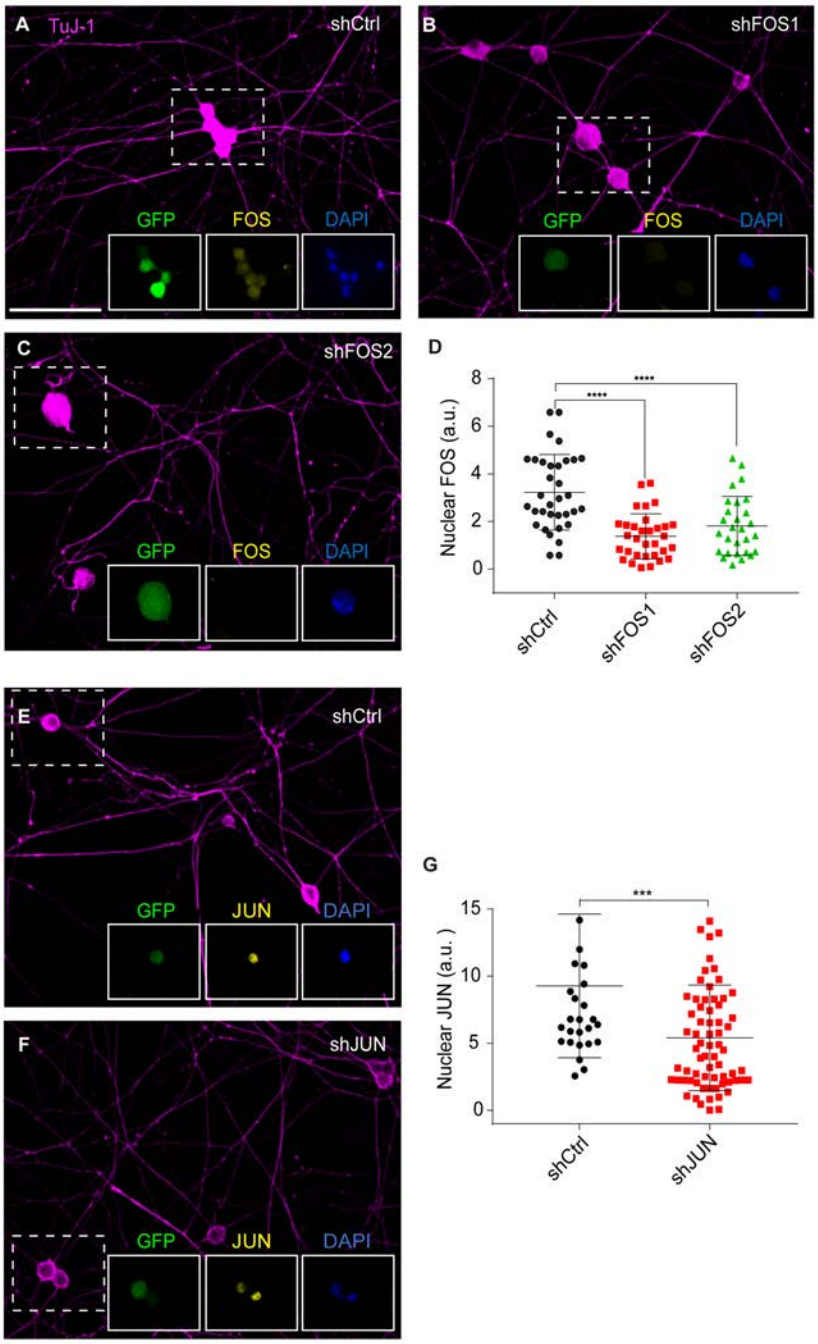

Fig. S8. Nuclear localization of c-Fos or c-Jun in shRNA-treated neurons in culture. Nuclear localization of c-Fos (**A-D**) or c-Jun (**E-G**) quantified in cultured adult DRG neurons transduced with AAV9 expressing shRNAs as indicated. n > 28, scale bar 100μm, *** indicates p <0.001, **** indicates p < 0.0001, ANOVA followed by Tukey's multiple comparison test. Quantifications shown as mean +/- SEM.

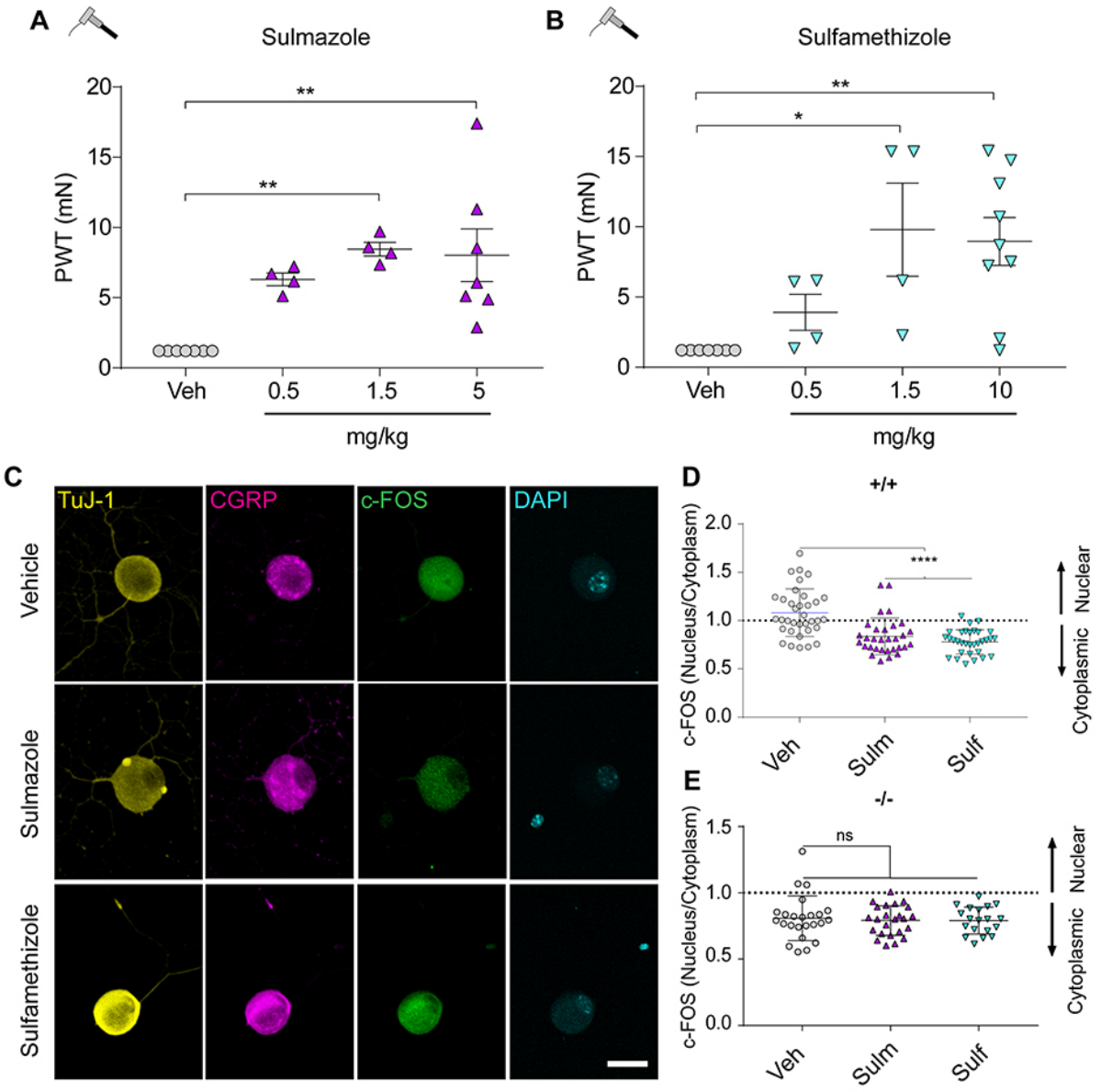

Fig. S9. Evaluation of the effects of sulmazole and sulfamethizole on mechanosensitivity and on c-Fos nuclear localization. Paw withdrawal threshold was assessed by the von Frey test one hour after drug treatment. Animals were injected i.p. one week after establishing SNI with the indicated concentrations of sulmazole (**A**) or sulfamethizole (**B**). n ≥ 4, * indicates $p < 0.05$, ** indicates $p < 0.005$, Kruskal-Wallis followed by Dunn's multiple comparison tests. All data shown as mean ± SEM. (**C, D**) Significant reductions in c-Fos nuclear localization (expressed as nucleus/cytoplasmic intensity ratio) in DRG neurons cultured after sciatic nerve injury of wild-type mice treated with sulmazole or sulfamethizole, compared to vehicle. Scale bar 25 µm. (**E**) No differences in c-Fos nuclear localization in importin α3 null DRG neurons treated as indicated. n > 31 neurons for each treatment. * indicates $p < 0.05$, ** indicates $p < 0.01$, **** indicates $p < 0.0001$, ANOVA followed by Tukey's multiple comparison test. Data shown as mean ± SEM throughout.

Captions for Tables and Movies:

Table S1. Differentially Expressed Genes from RNA-seq on importin α3 mice subjected to SNI.

RNA was extracted from adult DRG from wild type and importin α3 KO mice: Naïve, 7 days and 11 weeks after SNI. 1617 genes were found to be differentially expressed in at least one pairwise comparison. 530 genes were significantly differentially expressed ($p$adj ≤ 0.05, log2FoldChange ≥ 1 and max count ≥ 30) when comparing KO 7 days versus KO 11 weeks.

Table S2. CMap Analysis for compounds with transcriptome effects similar to importin α3 KO DRG

CMap analyses were conducted on differentially expressed gene-lists generated from comparisons of wild type importin α3 KO DRG. 101 compounds were detected with CMap scores ≥ 0.75.

Movie S1. Assessment of spontaneous coping behavior.

The video file contains three consecutive movies (2 minutes each) featuring mice from (1) 7 days after injury, (2) AAV-PHP.S-shCtrl 12 weeks after SNI, and (3) AAV-PHP.S-shα3 12 weeks after SNI, all monitored for spontaneous licking of the injured paw.